Interactions of Liquid Crystal-Forming Molecules with Phospholipid Bilayers Studied by Molecular Dynamics Simulations

Evelina B. Kim, Nathan Lockwood, Manan Chopra, Orlando Guzmán, Nicholas L. Abbott, and Juan J. de Pablo
Department of Chemical Engineering, University of Wisconsin, Madison, Wisconsin

ABSTRACT Recent experiments have shown that liquid crystals can be used to image mammalian cell membranes and to amplify structural reorganization in phospholipid-laden liquid crystal-aqueous interfaces. In this work, molecular dynamics simulations were employed to explore the interactions between commonly used liquid crystal-forming molecules and phospholipid bilayers. In particular, umbrella sampling was used to obtain the potential of mean force of 4-cyano-4′-pentylbiphenyl (5CB) and 4′-(3,4-difluor-phenyl)-4-pentyl-bicylohexyl (5CF) molecules partitioning into a dipalmitoylphosphatidylcholine bilayer. In addition, results of simulations are presented for systems consisting of a fully hydrated bilayer with 5CB or 5CF molecules at the lowest (4.5 mol %) and highest (20 mol %) concentrations used in recent laboratory experiments. It is found that mesogens preferentially partition from the aqueous phase into the membrane; the potential of mean force exhibits highly favorable free energy differences for partitioning ($-18\ k_BT$ for 5CB and $-26\ k_BT$ for 5CF). The location and orientation of mesogens associated with the most stable free energies in umbrella sampling simulations of dilute systems were found to be consistent with those observed in liquid-crystal-rich bilayers. It is found that the presence of mesogens in the bilayer enhances the order of lipid acyl tails, and changes the spatial and orientational arrangement of lipid headgroup atoms. These effects are more pronounced at higher liquid-crystal concentrations. In comparing the behavior of 5CB and 5CF, a stronger spatial correlation (i.e., possibly leading to aggregation) is observed between 5CB molecules within a bilayer than between 5CF molecules. Also, the range of molecular orientations and positions along the bilayer normal is larger for 5CB molecules. At the same time, 5CF molecules were found to bind more strongly to lipid headgroups, thereby slowing the lateral motion of lipid molecules.

INTRODUCTION

Molecular simulations have proven to be a useful tool for study of the interactions between a number of biologically relevant compounds and model cell membranes. A partial list of these chemicals includes toxic additives (such as pentachlorophenol (1)), anesthetics (such as halothane (2)), alcohols (such as methanol and ethanol (3)), cryopreserving agents (such as trehalose (4,5) and dimethylsufoxide (6,7)), and sterols and their derivatives (8–14). Simulations have been used to describe the elastic properties of membranes, the binding of biomolecules to phospholipid membranes, and the partitioning of various compounds from aqueous phase to membranes (for a review see Tieleman et al. (15) and references therein). In general, these simulations have revealed details pertinent to molecular/atomic level processes that are not easily accessible to experiments.

Liquid crystals (LC) have been proposed for imaging biologically relevant processes such as lipolysis at biomimetic interfaces (16) and cellular membranes (17). A nematic liquid crystalline phase exhibits long-range orientational order; the particular orientation induced by an interface (also known as surface anchoring) is extremely sensitive to the architecture and chemistry of the molecules at the interface (e.g., number of tails in a surfactant, the presence and length of double bonds in the lipid tails, the charge and size of the headgroup, etc.). Due to the nematic order, the orientation induced by an interface extends into the bulk over tens of micrometers; minute changes at an interface therefore give rise to optical textures that are easily detected through a polarizing microscope (18–20). Through this process, liquid crystals can be used to report the structural reorganization of a cellular or biomimetic membrane associated with adsorption or chemical reactions at an interface (16,21,22).

Recent experiments by Luk et al. (23) have considered the toxicity of several liquid crystal molecules (also called mesogens) with distinct chemical functional groups on live mammalian cells; their results indicate that 5CB, the most commonly studied liquid crystal former, is toxic to cells. Furthermore, it melts into the isotropic phase at 35°C, which is slightly below physiological temperature. On the other hand, a mixture of molecules whose rigid rod-like body is composed of difluorophenyl and bicyclohexane groups (the ''C'' series and ''TL205'') was found to be benign to the cells and, in fact, enhanced the cells' viability relative to the regular cell medium. (The latter finding was explained by a hypothesized enhanced oxygen solubility similar to that of perfluorinated alkanes used in blood substitutes.) Although this study identified a number of toxic and benign LC-forming compounds based on their functional chemical groups, and correlated the latter with toxicity, the mechanism by which 5CB is toxic to living cells was not established.

Submitted April 25, 2005, and accepted for publication June 13, 2005.

Address reprint requests to Juan J. de Pablo, Dept. of Chemical Engineering, University of Wisconsin, Madison, WI 53706. E-mail: depablo@engr.wisc.edu.

0006-3495/05/11/3141/18 $2.00

doi: 10.1529/biophysj.105.065193

A series of experiments by Kühnau et al. (24,25) on a system of dipalmitoylphosphatidylcholine (DPPC) mono- and bi-layers and 5CB revealed that 5CB was able to penetrate into a DPPC monolayer for areas per molecule higher than 0.48 nm^2. For this condition (at a temperature of 20°C), DPPC molecules are arranged in a tilted gel phase; 5CB annihilates the tilt and gives rise to a perfect homeotropic alignment of 5CB. In addition, the area-surface pressure isotherm of pure 5CB provides an estimate of the cross-sectional area of a mesogen at 0.4 nm^2—this is the collapse area of a pure 5CB monolayer at the air-water interface. After differential scanning calorimetry (DSC) measurements of DPPC multilamellar vesicles with 5CB incorporated at various concentrations, the authors concluded that 5CB reduces the size of ''cooperative units'' of phospholipids, thus giving rise to a broadening of the main and pretransition DSC signals for phase changes from liquid crystalline to ripple to gel phases, and reducing the main transition temperature.

In this work, computer simulations have been used to examine the behavior of model cell membranes (DPPC bilayers) exposed to a toxic mesogen, 5CB (4-cyano-4′-pentylbiphenyl), and nontoxic mesogens, 5CF (4′-(3,4-difluoro-phenyl)-4-pentyl-bicyclohexyl) and 3CF (4′-(3,4-difluoro-phenyl)-4-propyl-bicyclohexyl). The experiments on small unilamellar vesicles reported by N. Lockwood, A. Surjosantoso, E. B. Kim, J. J. de Pablo, and N. L. Abbott (unpublished) were performed with 5CB and ''TL205''. The latter is Merck's trade name for a liquid crystal consisting of a mixture of cyclohexane-fluorinated biphenyls and fluorinated terphenyls (the exact chemical formulae and composition are confidential). The composition of ''C series'', another benign liquid crystal used in the Luk et al. study (27), is known: it is an equimolar mixture of 4′-(3,4-difluoro-phenyl)-4-pentyl-bicyclohexyl (aliased 5CF in this article) and 4′-(3,4-difluoro-phenyl)-4-propyl-bicyclohexyl (aliased 3CF in this article). This mixture, however, is less readily available than TL205. The fluorinated phenyl group common to both C series and TL205 appears to be associated with nontoxicity to biological cells. We therefore chose to study the C series (i.e., an equimolar mixture of 5CF and 3CF) in this work; for simplicity, throughout the remainder of this article we designate C series and TL205 as 5CF/3CF or simply CF without any distinction. Preliminary experimental results suggest that both 5CB and 5CF/3CF diffuse from the bulk into DPPC small unilamellar vesicles upon long-term exposure. It is also found that incorporation of the LC into the membranes at various concentrations decreases the temperature at which the phase transition from gel to L_α fluid phase occurs. Measurement of the mesogens' solubility in water by ultraviolet (UV) absorbance revealed micromolar concentrations of 5CB in the aqueous phase; the presence of 5CF in water could not be detected by UV absorbance.

Our study begins by considering the partitioning of an individual mesogen into the membrane. The potential of mean force (PMF) of a LC molecule being pulled through a phospholipid bilayer is calculated using umbrella sampling techniques. Next, we explore the structure of LC-laden membranes. These simulations complement ongoing experimental investigations where DPPC vesicles with 5CB and 5CF at various concentrations were studied by DSC: the concentrations chosen for the simulations coincide with the lowest and highest concentrations used in experiments. The PMFs from the umbrella sampling simulations correspond to experiments where pure DPPC vesicles were exposed to bulk liquid crystal and again studied with DSC to detect any permeation into the membrane.

This investigation cannot be expected to resolve unambiguously the origins of 5CB toxicity, as we do not consider possible interactions with proteins and other inclusions in the cellular membranes. Nonetheless, we are in position to describe several general effects of 5CB and 5CF on membrane structure and, therefore, evaluate the possibility that mechanical damage to cellular membranes could contribute to cell death. Interestingly, cholesterol, an essential component of eukaryotic plasma membranes, is also a mesogen that forms a chiral nematic liquid crystalline phase under suitable conditions. A mixture composed of cholesterol derivatives, i.e., chloride, dichlorophenyl, and carbonate groups substituted at the hydroxyl position, was one of the eight LC-forming compounds tested in the toxicity study of Luk et al. (23). Clearly, there are interesting similarities between the widely studied cholesterol and the two molecules examined here, and we therefore present a comparison between the effects of these three liquid crystals on the same model membrane.

The outline of this article is as follows. In Molecular Dynamics Simulations we describe the methods and details of the models used in molecular dynamics simulations of fully hydrated DPPC bilayers with 5CB or 5CF. In Results and Discussion, we present the PMF for transfer of 5CB and 5CF molecules from an aqueous phase to a lipid phase using an umbrella sampling technique. We examine the effects that each molecule has on the structural properties of the membrane, including the ordering of lipid tails and the specific interactions with the headgroup of the phospholipids. Several concluding remarks are presented in Conclusions.

MOLECULAR DYNAMICS SIMULATIONS

We have simulated lipid bilayer systems consisting of 128 DPPC molecules, i.e., 64 lipids in each leaflet in the presence of water and 5CB/5(3)CF molecules (see Fig. 1). Initial bilayer configurations were generated by placing the DPPC and water molecules on a regular grid. Additional components were randomly interspersed in the bilayer, with an equal number of molecules in each leaflet; the polar atoms of the cyano group in 5CB and fluorine atom in the *para* position in CF were placed at roughly the same height as the ester groups of the lipid fatty acids. After a brief compression at 100 K and 10 bar to the cell size that approximately

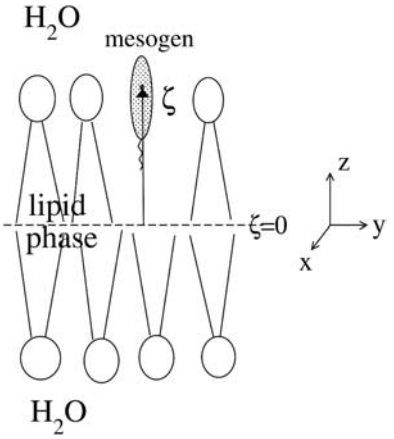

FIGURE 1 Definition of the reaction coordinate ζ for umbrella sampling simulations. Phospholipids are shown schematically as headgroups with two acyl chains, assembled in a bilayer (*lipid phase*) in contact with the aqueous phase; ζ is defined as the distance in the z direction from the bilayer center ($\zeta = 0$) to the C8 (5CB) or C7 (5CF) sites in the liquid crystal molecules (see Fig. 2).

corresponds to a simulation cell for a pure DPPC bilayer (4), the systems were equilibrated at 350 K and 1 bar for at least 10 ns. An additional 20 ns were used to generate data for subsequent analysis. The compositions of the simulated systems are listed in Table 1. The molar LC/lipid ratios of 1:21 and 1:4 for both mesogens match the lowest and highest concentrations tested in our experiments.

For free energy calculations (i.e., single mesogen systems), we employed a smaller system consisting of 80 lipids (40 per leaflet) and 2664 water molecules. Configurations for these simulations were equilibrated for 10 ns and production runs were 20 ns long, with a simple harmonic umbrella potential ($k^{\mathrm{umb}} = 500$ kJ/mol/nm^2) imposed on the C8 and C7 sites of 5CB and 5CF molecules, respectively (see Fig. 2). The harmonic potential for each simulation was centered at $z^{\mathrm{eq}} = z(\mathrm{DPPC}) - z(\mathrm{C7\ or\ C8}) = 0, 0.25, 0.45, 0.7, 0.95, 1.15, 1.35, 1.55, 1.8, 2.0, 2.2$ (2.3 for 5CF), 2.4, 2.65, 2.9, 3.2, 3.5, and 3.8 nm, where z(DPPC) is the z-coordinate of the center of mass of DPPC molecules. For cases in which a mesogen was protruding or fully immersed into the aqueous phase, extra water was added (3540 molecules total) to eliminate the interaction with the periodic image of the opposite leaflet of the bilayer (by effectively increasing the height of the slab of bulk water from 1 to 1.5 nm). The augmented system was used for $z^{\mathrm{eq}} \geq 2.9$ nm in the case of 5CB and for $z^{\mathrm{eq}} \geq 2.3$ nm in the case of 5CF.

TABLE 1 Composition of simulated lipid bilayer systems

System	5CB	5CF/3CF	LC concentration*
5CB-L	6	—	1.5 wt %/4.5mol %
5CB-H	32	—	8.2 wt %/20 mol %
CF-L	—	3/3	2.1 wt %/4.5 mol %
CF-H	—	16/16	21.9 wt %/20 mol %

All simulations contained 128 lipids and 3655 water molecules.
*Water-free basis.

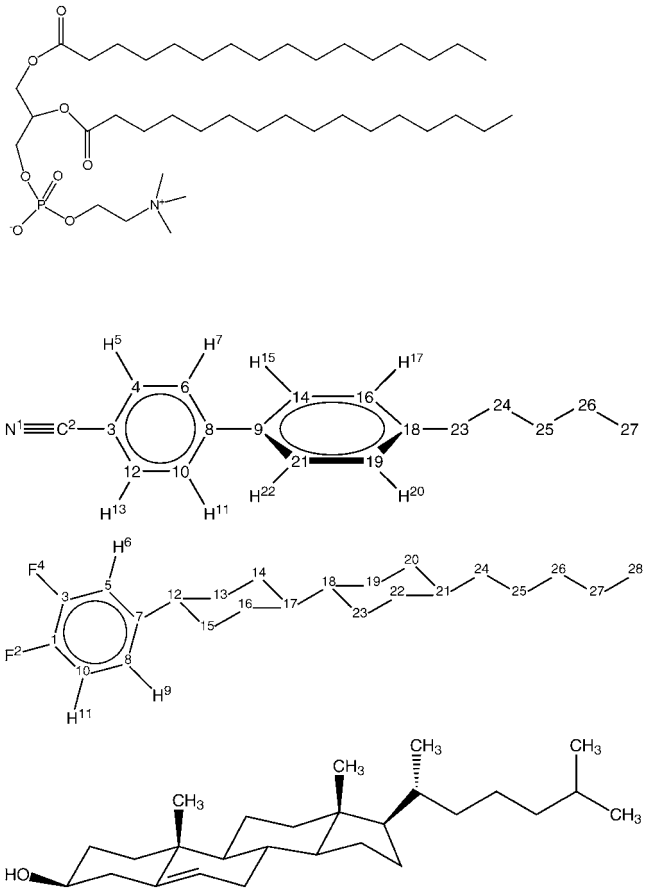

FIGURE 2 Molecular structures of (*top* to *bottom*) DPPC, 5CB, 5CF, and cholesterol. The lengths of the rigid parts of the molecules (in the same order) are 1.08 nm (N1–C23), 1.43 nm (F2–C24), and 1.28 nm (hydroxyl H–C22).

Constant pressure-constant temperature molecular dynamics simulations were performed with Gromacs (28). We employed a leapfrog integration algorithm with a 2 fs time step; temperature and pressure were kept constant through a weak coupling technique (29) with correlation times $\tau_{\mathrm{T}} = 0.2$ and $\tau_{\mathrm{P}} = 2.5$ ps for temperature and pressure, respectively. The three sides of a rectangular simulation box were allowed to fluctuate independently and were coupled to a pressure bath at 1 bar with a compressibility of $\kappa = 0.46 \times 10^{-6}$ kPa^{-1}. A particle-mesh Ewald method (30) was used to calculate the long-range electrostatic interactions. Nonbonded interactions were cut off at 0.9 nm. The bond lengths were kept constant by applying the LINCS algorithm. The simulation parameters are identical to those of Sum et al. (4) except for the use of the reaction field correction to account for the long-range electrostatic interactions.

For water and DPPC, we used the same models as in Sum et al. (4): SPC/E for water (31) and a force field assembled from various sources for lipids, i.e., GROMOS for the headgroups (32), and NERD for the aliphatic tails (33–35).

To model 5CB and 5CF (their molecular structures are shown in Fig. 2), we again resorted to a combination of united-atom type force fields for the aliphatic parts of a molecule (i.e., saturated hydrocarbon chains (33–35) and cyclohexane rings (36)) and previously developed all-atom models for molecular fragments most commonly encountered in thermotropic liquid crystals, i.e., cyanobiphenyl and fluorophenylcyclohexane (37). In this manner, we achieve consistency with the lipid molecules model on the one hand, and efficiency through a reduced number of explicit hydrogen atoms on the other hand. Such combination has been successfully employed in molecular simulations of the smectic phase of 8CB (38). It must be noted that the explicit inclusion of hydrogen atoms in the biphenyl group is important to properly represent the misalignment of the planes of the rings (39): the π-electrons on the two rings have a propensity to align those, whereas the steric repulsion between hydrogens in positions 7, 11, 15, and 22 tends to misalign the planes. In a fluorophenyl group of 5CF, both hydrogen and fluorine atoms are included explicitly as well.

The force field parameters for the mesogenic fragments, i.e., cyanobiphenyl and difluorophenyl, were taken directly from Cheung et al. (37). These include bond lengths (stretching), bond angle bending, proper and improper dihedral torsion (the latter is required to keep the rings planar), and Lennard-Jones parameters. In addition, we adopted Cheung's partial charges for cyanobiphenyl; for the 3,4-difluorophenylcyclohexane fragment we computed partial charges due to a significant difference with the 2-fluorophenyl fragment for which Cheung's force field was originally developed. The charges were determined by Gaussian 98 calculations (40) with MP2/6-31G(d) basis functions and are reported in Table 2.

The intra- and intermolecular interaction parameters for 5CB were then assembled from Cheung et al. potential and NERD. For 5CF, the set (already containing parameter subsets for 3,4-difluorophenyl (37), cyclohexyl (36), and acyl chain (33)) had to be completed by determining the additional parameters for dihedral torsion between 3,4-difluorophenyl and cyclohexyl and between two cyclohexyl groups. These parameters were determined by Gaussian calculations with MP2/6-31G(d) basis functions and are reported in Table 3. For completeness, we list the force field parameters for the cyclohexyl groups from Neubauer (36) in Table 4; these parameters are similar to those from NERD.

Note that, unlike in the NERD force field, where 1-4 nonbonded interactions are excluded, the 1-4 nonbonded interactions in all-atom description are scaled by a factor of a half and an eighth for the van der Waals and Coulombic terms, respectively. To resolve this difference, the scaling was applied to all 1-4 pairs when at least two of the four atoms belonged to a phenyl ring, i.e., a molecular fragment with all atoms explicitly modeled. For example, in 5CB, the interactions between C16 and methylene 24 were scaled, whereas no 1-4 interactions were accounted for between sites 18 and 24. Similarly, in 5CF, pairs 5-15 and 8-15 were scaled, but not 7-13 or 7-15.

TABLE 2 Calculated partial charges for difluorophenylcyclohexyl

Site*	Charge†	Site	Charge
C1	+0.328	C8	−0.250
F2	−0.303	H9	+0.182
C3	+0.332	C10	−0.192
F4	−0.305	H11	+0.200
C5	−0.288	C12	−0.054
H6	+0.197	C13/C15	+0.017
C7	+0.103	C14/C16	+0.006
C17	+0.004		

Atom numbering is as defined in Fig. 2. For comparison, partial charges on 5CB atoms as adopted from Cheung et al. (37) are −0.43 (N1), +0.395 (C2), +0.035 (C3), +0.122 (all phenyl ring hydrogens), and −0.122 (all phenyl ring carbons except C3, C8, and C9).
*C in cyclohexyl refers to united carbon and hydrogen sites.
†Units of electron charge.

RESULTS AND DISCUSSION

Potential of mean force for mesogen insertion into the bilayer

A DPPC molecule consists of a glycerol backbone to which two 16-carbon acyl chains and a headgroup (containing negatively charged phosphate and positively charged choline groups) are attached through ester links (Fig. 2). The average positions of carbonyl, phosphate, and choline groups in a bilayer are convenient landmarks to define the position of a membrane inclusion. We define a reaction coordinate ζ as the distance along the bilayer normal from the bilayer center to a specific site in the mesogens, C8 in 5CB and C7 in 5CF. That is, in practice we impose a simple harmonic umbrella potential on these particular sites and thus restrain movement of the entire molecule. The reasons behind our choice of the reaction coordinate ζ stem from the fact that the mesogens under consideration have the shape of a rigid cylinder with a high aspect ratio. Restraining a site in the middle of a molecule makes visualization of the orientational conformations easier (a rigid rotation around a fixed point). As

TABLE 3 Parameters for inter-ring proper dihedral torsional potential for difluorophenylcyclohexyl (first three columns) and cyclohexyl-cyclohexyl rings (last two columns)

i	V_i (kJ/mol)	ϕ_{eq} (°)	V_i (kJ/mol)	ϕ_{eq} (°)
0	7.911	0	16.282	0
1	−0.096	297	−8.345	56
2	−7.242	234	5.053	112
3	−0.262	171	−14.334	168
4	0.676	108	0.606	224
5	0.132	45	−1.598	280
6	−1.200	342	2.248	336
7	—	—	0.057	32

The torsional potential is of the form $E_{tor} = \sum_{i=0}^{n} V_i[1+\cos(i\phi - \phi_{eq})]$.

TABLE 4 Force-field parameters for cyclohexyl rings

Lennard-Jones parameters	$\varepsilon = 50.37$K
	$\sigma = 0.393$ nm
Fixed bond length	$l_{eq} = 0.15320$ nm
Harmonic angle bending	$k_\theta = 62500$ K/rad^2
Equilibrium bond angle	$\theta_{eq} = 111.8°$

Values in the table were adopted from Neubauer et al. (36). The torsional potential parameters are identical with NERD (33).

these rigid molecules are pulled through a membrane, their orientation distribution is constrained dramatically. Hence, the region of phase space sampled by a mesogen is reduced and an accurate estimation of the system free energy is possible in relatively short simulations. Since we integrate out the orientational degrees of freedom (by not restricting molecular orientations), the accuracy of the PMF is highly dependent on the efficiency of the sampling of the mesogens' orientational phase space.

As detailed in Molecular Dynamics Simulations, in umbrella sampling multiple independent simulations are performed in which a mesogen site is forced (via an umbrella potential) to sample a limited range of depths in the bilayer in the vicinity of a chosen depth, z^{eq}. The sampled range of ζ depends on the imposed umbrella potential. A distribution of sampled depths is collected in a histogram for each umbrella. At the end of a simulation, the effect of the biasing potential is removed. The final histograms collected for each umbrella are reweighed using a weighted histogram analysis method (41), thereby generating a global distribution in the reaction coordinate $g(\zeta)$ and the free energy $\Delta G(\zeta) = -k_B T \ln [g(\zeta)]$.

Fig. 3 shows the free energy profiles corresponding to the transfer of a mesogen from the aqueous to the lipid phase. The upper panels of the graphs map the locations of various system components through their mass density profiles along the bilayer normal. Several common features of the PMF for both molecules are apparent: the free energy change for partitioning into a membrane, that is, the difference between the free energies at $\zeta \to \infty$ and at the value of ζ corresponding to the lowest free energy inside the bilayer, favors inclusion into the bilayer and is estimated to be -53 kJ/mol ($-18\ k_B T$) for 5CB and -76 kJ/mol ($-26\ k_B T$) for 5CF. A global minimum in the free energy at 0.8 and 1.1 nm for 5CB and 5CF, respectively, reveals a preferred location for C8 and C7 sites. In both PMF profiles, four distinct regions can be clearly identified: 1), the bilayer middle region, which gives rise to an energy barrier for crossing from one leaflet to the other; 2), a stable region around a free energy minimum; 3), the region of steep gradient or large attractive force pulling a mesogen toward the bilayer; and 4), the aqueous phase region farthest from the bilayer center, where the PMF is flat and, hence, no interaction between mesogens and the bilayer is evident (this also corresponds to the reference state where free energies were arbitrarily set to zero). We now discuss these regions in more detail.

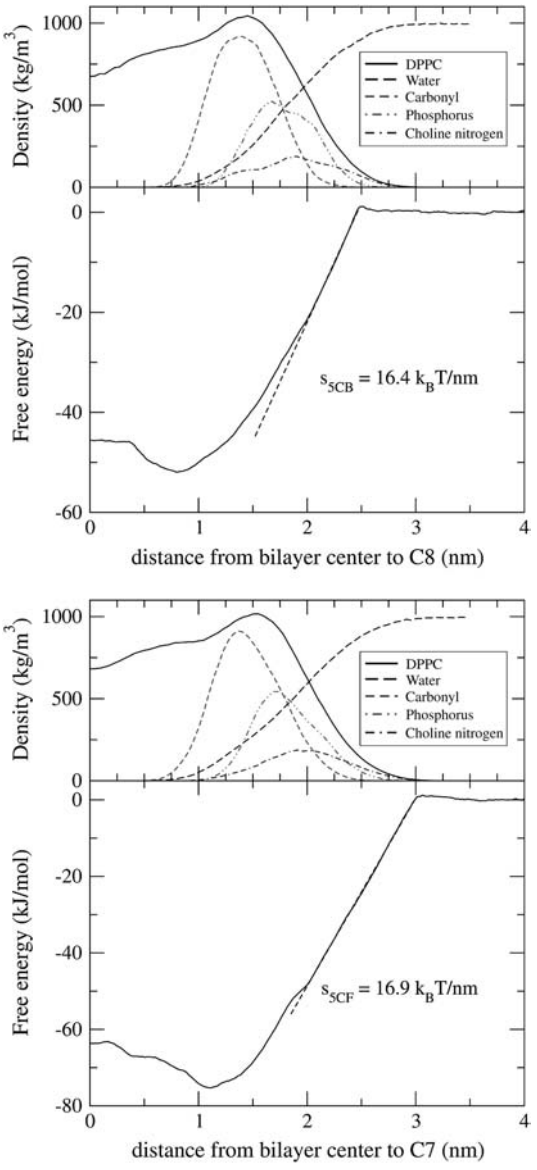

FIGURE 3 PMF of transfer for 5CB (*top*) and 5CF (*bottom*) molecules from aqueous to lipid phase. The curves were obtained by reweighing umbrella sampling histograms with a weighted histogram analysis method (41; see text for details). The upper panels show bilayer density profiles of various system components. DPPC (*solid line*), water (*long-dashed line*), carbonyl (*short-dashed line*), phosphorus (*double-dot-dashed line*), and choline nitrogen (*double-dash-dotted line*); the latter three were scaled by a factor of 5 for clarity.

As pointed out previously, mesogen orientations are intimately correlated with their location in the membrane and, therefore, with the bilayer structure (as measured by the density profiles in Fig. 3) and the resulting free energies. To facilitate our discussion, in Fig. 4 we present the distribution and mean values of the angles between the vectors characterizing mesogen orientation and the bilayer normal. In region 1, defined by $\zeta < 0.44$ nm for 5CB ($\zeta < 0.6$ nm for 5CF), the PMF is relatively flat and is higher than the global minimum

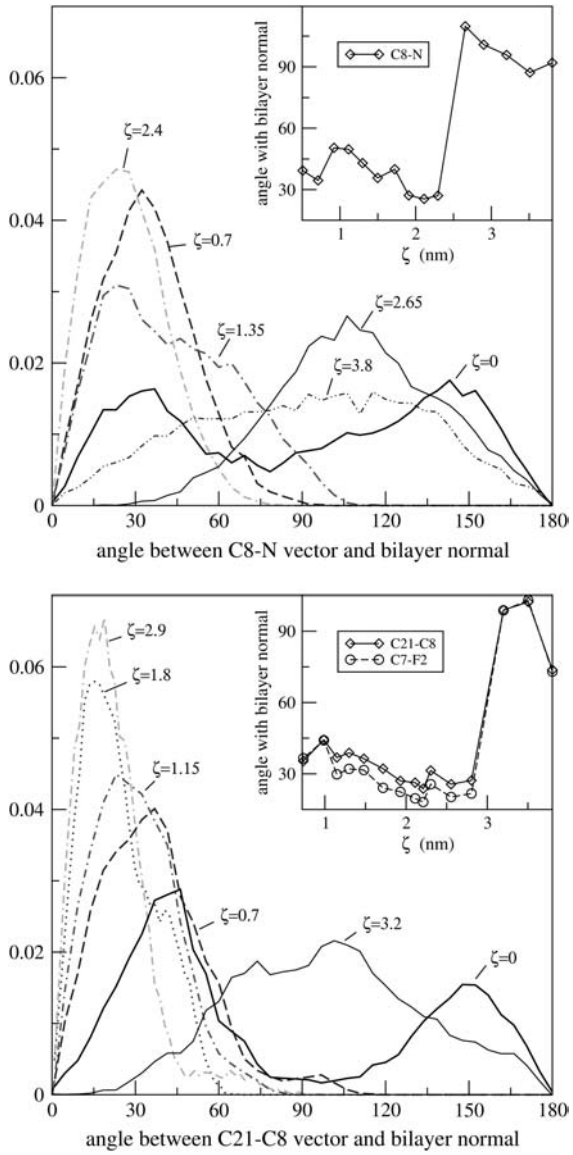

FIGURE 4 Molecular orientation distribution at selected values of the reaction coordinate (as indicated on the graphs) in lipid and aqueous phases for 5CB (*top*) and 5CF (*bottom*). The insets show the average molecular tilt as a function of the distance from the bilayer center.

by 8 kJ/mol (13 kJ/mol). This means that mesogens must overcome an energy barrier of ~2.7 k_BT (4.5 k_BT) to cross from one leaflet into another. It has been argued from free volume considerations that small organic molecules would partition into the middle of the bilayer, also called methyl trough, where the lipid density is lower. The free energies are negative with respect to the aqueous phase for transfer of ethanol and benzene (42) and a slight dip in free energy is present for a water molecule in the same lipid region (42–44). This is not the case for the mesogens considered here, for which molecular volumes and lengths exceed the extent of the methyl trough region of the membrane. However, if a molecule aligns perpendicular to the bilayer normal within the methyl trough the free energies could be lowered. From Fig. 4 it can be seen that a significant fraction of the orientations that 5CB adopts when restrained at $\zeta = 0$ is ~90°. In general, the orientational distribution is rather wide, with a favored tilt of 35° and 145°. The indifference to the molecular orientation is observed in a flat stretch of the PMF for 5CB in region 1. Similarly, 5CF exhibits a bimodal distribution in the angle it makes with the bilayer normal. The peaks at 35° and 150°, however, are much more pronounced. The examination of the trajectories at $\zeta = 0$ revealed that although the 5CB orientation flipped (from pointing toward the headgroup regions of different leaflets) at least four times during the simulation, i.e., the average time between the flips is 5 ns, 5CF molecular vectors flipped only once throughout 20 ns of production simulation time. The rearrangement of the lipids surrounding a 1.4-nm-long 5CF molecule for this type of motion requires significantly more energy than that required for a shorter 5CB molecule. The bimodal distribution persists for both molecules throughout region 1 until $\zeta \approx 0.5$ and $\zeta \approx 0.73$ nm for 5CB and 5CF, respectively.

Region 2, where molecules exhibit the lowest free energies, corresponds to $\zeta = 0.8 \pm 0.4$ nm for 5CB and $\zeta = 1.1 \pm 0.4$ nm for 5CF. The average orientation of the molecular vectors for this region is shown in the insets of plots in Fig. 4. The orientational distribution curves at the free energy minimum correspond to those marked as $\zeta = 0.7$ nm for 5CB and $\zeta = 1.15$ nm for 5CF in Fig. 4. Using the average 5CB tilt angle of 35°, we can calculate the average position of a cyano nitrogen as 1.24 nm above the bilayer midplane. This is ~0.2 nm below the average position of lipid carbonyl groups (1.44 ± 0.02 nm). For comparison, the lipid phosphorus and nitrogen atoms are on average located 1.81 ± 0.02 nm and 1.92 ± 0.02 nm from the bilayer midplane. For 5CF, the average location of the F2 site is 1.44 nm, i.e., 0.09 nm above that of the lipid carbonyl groups; however, the standard deviation in the distance between carbonyl groups is 0.1 nm. The lipid phosphorus and nitrogen atoms are located at 1.75 ± 0.11 nm and 1.85 ± 0.17 nm, respectively. At the same time, the positions of the (united) carbon atoms marking the end of the rigid part of a molecule, C18 in 5CB and C21 in 5CF, are 0.47 nm and 0.37 nm. That is, the ringed rigid parts of the mesogens are contained in the part of the membrane between the methyl trough and the carbonyl groups of the lipids, whereas the flexible aliphatic tails are preferentially located within the methyl trough. The same configuration has been reported for cholesterol molecules (8,9,12). It must be noted, however, that the tilt angle and the average positions of the molecules change slightly when their concentration in the bilayer is higher. In general, the calculated locations of mesogen polar atoms relative to DPPC polar atoms in simulations with a single mesogen agree well with those observed in simulations of LC-rich bilayers.

Region 3 in the PMF profile corresponds to $1.25 < \zeta < 2.5$ nm for 5CB and $1.5 < \zeta < 3.0$ nm for 5CF. A large free

energy gradient in this region corresponds to a large force opposing the mesogen's motion out of the bilayer. Initially, as the mesogen penetrates the headgroup region of the membrane, it has to make space for itself by pushing lipid headgroups aside. A bilayer is stabilized by a balance between headgroup and chains' pressure to expand and the interfacial pressure to shrink laterally to minimize the exposure of the hydrophobic part of the membrane to water (45); insertion of a mesogen's cyanophenyl or fluorophenyl group in the lipid headgroup region has an unfavorable effect since it restricts the in-plane motion of lipid headgroups and creates additional interface between the hydrophobic bilayer interior and hydrophobic mesogenic fragments and water. There is a clear shift in the average tilt angle of the mesogens, as seen in Fig. 17. Being more mobile, 5CB is orientationally destabilized, as exemplified by a wide angular distribution (see curve for $\zeta = 1.35$ in Fig. 4, *top*). A longer 5CF molecule slowly reorients from a previously favored tilt angle of 40° to an angle of 15°: this can be observed in the curve for $\zeta = 1.8$ of Fig. 4, *bottom*, where a main peak at 15° and a residual shoulder at 40° are clearly visible. Once the first phenyl ring of either mesogen is inserted in the lipid headgroup region, the tilt angle is the closest to the bilayer normal and the angular distribution is narrow. From this point on, the unfavorable free energy is a result of the hydrophobic effect (46) that arises from changes in van der Waals interactions and the structure of water in the presence of a hydrophobic mesogen.

It is instructive at this point to refer to a study of the interactions of cholesterol with lipid bilayers by continuum-solvent theoretical methods conducted by Kessel et al. (47). By approximating a hydrated lipid bilayer as a slab with low dielectric constant ($\varepsilon_{lip} = 2$), surrounded by a solvent of high dielectric constant ($\varepsilon_{wat} = 80$), the authors computed the PMF for a cholesterol molecule at a fixed (and most favorable) orientation as a function of the cholesterol penetration depth into the bilayer. The nonpolar contribution, ΔG_{np}, is more important when the cholesterol molecule is displaced from the minimum, out of the bilayer into the aqueous phase. They calculated $\Delta G_{np} = \tilde{\gamma}A + \tilde{b}$, where A is the water-accessible surface area of cholesterol, $\tilde{\gamma} \approx 4.7\, k_BT/\text{nm}^2$ is the surface tension, and $\tilde{b} \approx -2.9\, k_BT$. The latter values were derived from experiments on the partitioning of alkanes between water and liquid alkanes (48). They found ΔG_{np} to be proportional to the penetration depth ζ, with the proportionality coefficient $s_{chol} = 20\ k_BT/\text{nm}$. For the mesogens considered in this work, the assumption of linear dependence of the free energy on the z-location in the bilayer agrees well with our PMF results in most of region 3 (especially for the higher values of ζ). As discussed above, the distribution of molecular orientations is relatively sharp around the average values (see curves $\zeta = 2.4$ for 5CB and $\zeta = 2.9$ for 5CF in Fig. 17), thereby rendering the comparison with Kessel's calculations valid in this region. We measured the initial slopes of the PMF curves and obtained $s_{5CB} = (d\Delta G(\zeta)/d\zeta)|_{\zeta\,=\,2.5} = 16.4\ k_BT/\text{nm}$ and $s_{5CF} = (d\Delta G(\zeta)/d\zeta)|_{\zeta\,=\,3.0} = 16.9\ k_BT/\text{nm}$. These values are similar to each other (a result of having molecules of similar shape and architecture) and are comparable to the estimate of $s_{chol} = 20\ k_BT/\text{nm}$. Also, note that the PMF curve for 5CB starts deviating from the linear fit after only 1 nm, as opposed to 2 nm for 5CF. This is caused by the higher orientational mobility of 5CB, as evidenced by wider angular distributions and by the shorter length of the molecule (see also Fig. 2). In addition, the minimum value of the PMF for cholesterol from Kessel et al. ($-25\ k_BT$) is of the same order of magnitude as our estimates of $-18\ k_BT$ and $-26\ k_BT$ for 5CB and 5CF, respectively.

Following the ideas of Kessel et al., if the shape of a mesogen is approximated by a cylinder of radius R, then the expression for the nonpolar contribution to the free energy can be rewritten as $\Delta G_{np} = 2\tilde{\gamma}\pi R\zeta + \tilde{b}$; the slope s of the PMF in region 3 can be expressed as $2\tilde{\gamma}\pi R$ and a rough estimate of the cross-sectional area of a molecule can be obtained. Using the same value for $\tilde{\gamma}$ as Kessel et al., we find $R_{5CB} \approx 0.56$ nm and $R_{5CF} \approx 0.57$ nm; the corresponding areas are 0.97 nm^2 and 1.03 nm^2. These estimates are too large; the measured cross-sectional areas of cholesterol and 5CB are 0.37 nm^2 and 0.40 nm^2, respectively (the latter was experimentally measured by Kühnau et al. (24) from the collapse pressure of a monolayer of pure 5CB in a Langmuir-Blodgett film). The assumption of circular molecular surface is too crude for these molecules. On the other hand, assuming the same area correction factor of 0.40 nm^2/0.97 nm^2 for 5CB, the corrected cross-sectional area of a 5CF molecule is 0.42 nm^2.

The transition from the lipid headgroup region (region 3) to the aqueous phase (region 4) is accompanied by a drastic change in molecular orientations, as shown in Fig. 4 (in particular, see the curves for $\zeta = 2.65$ and $\zeta = 3.8$ for 5CB and $\zeta = 3.2$ for 5CF). Note that, when the mesogens are still partially inserted in the bilayer (corresponding to $z^{eq} = 2.4$ for 5CB and $z^{eq} = 2.9$ for 5CF), the sites C18 in 5CB and C21 in 5CF are at the same depth as the lipid nitrogen atoms. It is the position of these molecular sites (i.e., the sites that mark the end of the rigid molecular bodies) that determines whether a mesogen will ''stand up'' partially inserted into the membrane or orient parallel to the bilayer surface fully immersed in water. Since the distance from C7 to C21 in 5CF is larger than the C8–C18 distance in 5CB (see Fig. 2), the value of ζ at which 5CF transitions to region 4 is higher than that for 5CB. Beyond these penetration depths, 5CB and 5CF adopt orientations such that the polar cyano or fluorine groups are closer to the lipid headgroups than the rest of the molecule, i.e., a tilt angle >90°. Upon further separation from the bilayer, 5CB and 5CF sample all angles uniformly. We observe the presence of a small, ~0.3 k_BT energy barrier for penetration into the bilayer. This process is associated with the loss of orientational freedom for mesogens and the loss of favorable electrostatic interactions between the polar atoms of the bilayer headgroups and the mesogen. Still, the liquid crystal is solvated by water and the free energy is

lowered through the elimination of unfavorable interactions between the mesogen's hydrophobic aliphatic tails and water.

Distribution of mesogens in an LC-rich bilayer

In this and subsequent sections, we turn to LC-rich bilayers. The pure bilayer system has been investigated before using precisely the same model (4). Note that the temperature chosen for this work is above the main gel-liquid crystalline transition of the bilayer.

The systems under consideration are designated as 5CB-L, CF-L, 5CB-H, and CF-H, where L and H stand for low and high LC concentrations (4.5 and 20 mol %, respectively) and CF denotes an equimolar mixture of 5CF and 3CF molecules (see also Table 1). In all systems the mesogens, initially placed inside the bilayer, did not segregate to the aqueous phase. To examine the large-scale motion of mesogens within a bilayer we have included in Fig. 5 the trajectories of a few selected molecules out of the 5CB-L and CF-H systems. It is apparent that molecules can cross from one leaflet to the other in the span of a nanosecond or longer.

The density profiles of the four systems considered in this work are shown in Fig. 6 (see also Fig. 8 for total LC densities). From the density profiles in Fig. 6 one can see that, on average, mesogens align in the bilayer consistently with the results from umbrella sampling simulation.

1. The polar end points toward the lipid headgroups and is located just below the average position of the lipid carbonyl groups.
2. The aliphatic chains are confined to the middle of the bilayer and coincident with the methyl trough.
3. The biphenyl and bicyclohexyl groups span the entire width of the bilayer, with the peaks located intermediate to the mesogen ''headgroups'' and their aliphatic chains.

The density peaks pertaining to mesogens are wide and asymmetric around the bilayer center, thus indicating relatively free orientational motion and movement from one leaflet to another. The asymmetry is higher in the 5CB systems, and is partially due to the propensity of these molecules to aggregate. Note also that the density of cyanophenyl (or fluorophenyl in CF-L) or phenyl (bicyclohexyl) is not identically zero in the middle of the bilayer. To examine this phenomenon more closely, in Fig. 7 we plotted the orientations that mesogens adopt depending on the position of the polar atoms (cyano nitrogen in 5CB or F2 in CF), along the bilayer normal during the last 5 ns of the simulation. In all systems, the highest density of data points is found within a range of positions along the normal that coincides with that spanned by the density peaks of cyanophenyl and difluorophenyl groups in Fig. 6. However, Fig. 6 also shows that a nonnegligible number of configurations exhibit depths in the bilayer all the way down to its middle. When a polar mesogen atom (cyano N or F2) is found closer to the middle

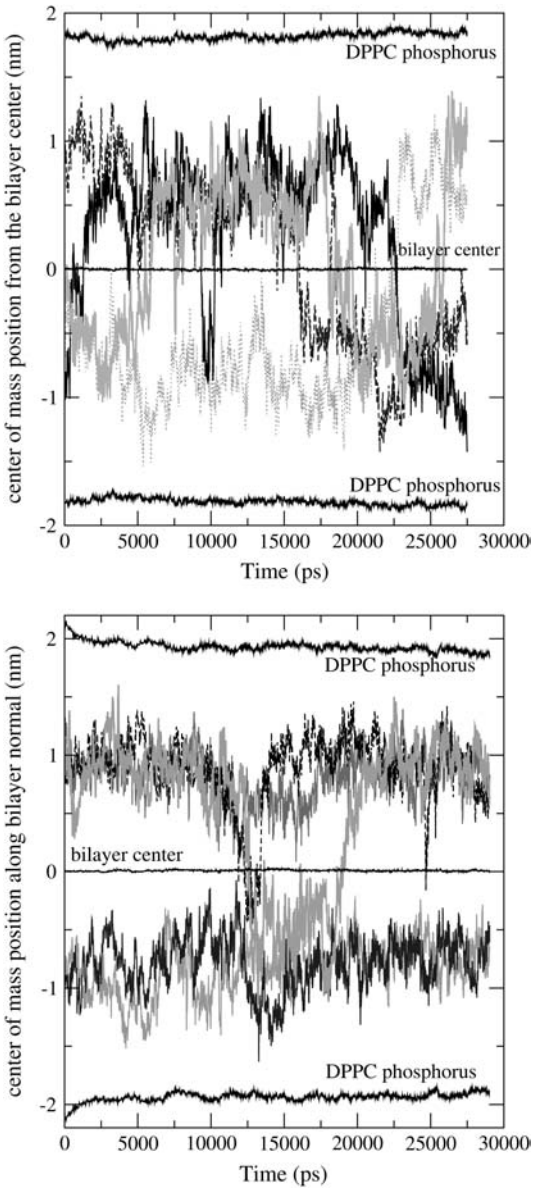

FIGURE 5 Trajectories of centers of mass of selected mesogens over the entire simulation time for 5CB-L (*top*) and CF-H (*bottom*) systems. The average positions of phosphorus atoms in each leaflet and of the bilayer center of mass are shown for reference.

of the bilayer, the corresponding molecular orientations are widely distributed—much more so than in the dense clouds—and even indicate the presence of molecules turned upside down (i.e., with their aliphatic tails close to the lipid headgroups). At both low and high concentrations, 5CB molecules seem to deviate more from the average position and orientation than CF molecules. This can be more clearly visualized for the CF-L system. This higher degree of disruption by 5CB may have consequences for the mechanical properties of the membranes. The orientational freedom experienced by the mesogens can be contrasted with the orientational confinement experienced by cholesterol

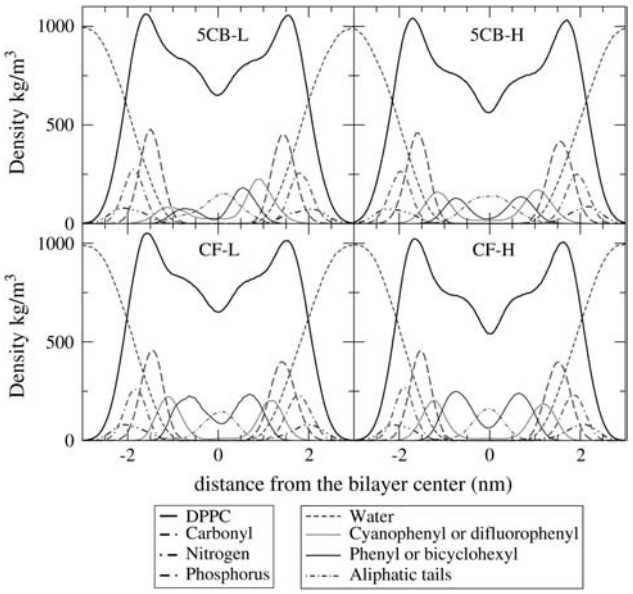

FIGURE 6 Density profiles for the systems listed in Table 1 as a function of the distance from the center of the bilayer (nm). Bold lines refer to lipid components: DPPC (*solid line*), carbonyl (*dashed line*), nitrogen (*double-dot-dashed line*), and phosphorus (*dot-double-dashed line*); regular lines refer to water (*dashed*), cyanophenyl or difluorophenyl groups (*solid gray*), phenyl or bicyclohexyl (*solid black*), and aliphatic tails (*dot-dashed*) for 5CB or CF systems, respectively. (For clarity, the densities of DPPC carbonyl, N, and P were scaled by a factor of 2; all mesogen component densities were scaled by 10 in low-concentration cases and by 2 in high-concentration cases.)

molecules in a DPPC bilayer: the data points of the tilt angle of cholesterol as a function of the *z*-position of its hydroxyl oxygen (9) fit into the rectangular areas highlighted in Fig. 7 (see 5CB-L and 5CB-H plots). Although the data for cholesterol correspond to 2 ns of simulation time (and to a lower temperature of 325 K), the reduction in the range of molecular tilt and *z*-positions of the cholesterol polar headgroup in comparison with those of 5CB and CF is drastic. With many more degrees of translational and orientational freedom, 5CB and CF molecules may be more disruptive to the membrane than cholesterol.

Another interesting feature of all plots in Fig. 7 is that there appears to be a diagonal border that marks the largest values of tilt angles sampled by the mesogens. This possibly signifies a so-called ''hydrophobic mismatch'' effect, when characteristic lengths of a membrane (e.g., thickness) and/or of an inclusion of a comparable size are adjusted in such a manner that the lengths of hydrophobic regions of both match. For example, in experiments where gramicidin was embedded in dilauroylglycerophosphocholine (DLPC) and dimyristoylglycerophosphocholine (DMPC) bilayers that in the absence of the peptide have thickness lower and higher than the length of gramicidin, respectively, the thickness of the membranes stretches or shortens according to the mismatch (49). In our case, neither mesogen is sufficiently long to induce a gramicidin-like effect; however, there must be a match between a characteristic length of a mesogen (the majority of its length can be considered hydrophobic) and a half-width of the membrane. Therefore, the closer the polar end of a mesogen is to the DPPC midplane, the higher its tilt angle has to be for the molecule to stay in the same bilayer leaflet.

At the same time, the response of the bilayer to the presence of mesogens is to thicken so as to accommodate a mesogen in a leaflet more easily and to increase favorable van der Waals (hydrophobic) interactions. In addition, the presence of a mesogen, a rigid, approximately cylindrical inclusion, hinders the lateral motion of the lipid chains and induces elastic deformations of the lipid chains, such as twist and splay. This again results in the elastic deformation of the membrane. As shown in Fig. 8, the bilayer width increases with increasing LC concentration. At low concentrations, the changes induced by the presence of the mesogens are virtually identical for 5CB and CF. On the other hand, CF impacts the system dimensions more than 5CB at the same molar concentration. For a reference, it is instructive to examine the distances between the density peaks of the components presented in Fig. 8—these are compiled in Table 5. For example, the distance between lipid phosphorus atoms increases from 3.52 nm for the pure bilayer to 3.79 nm (3.84 nm) for the 5CB-H (CF-H) system. This can be indirectly compared to a cholesterol induced increase of the same distance from 3.8 nm in a pure bilayer to 4.42 nm in a 50 mol % cholesterol-DPPC system (9). From purely geometric considerations, it is reasonable to expect that a longer CF molecule will stretch the bilayer thickness more to fit into the hydrophobic part of it.

Another feature of the tabulated distances is that phosphate and choline groups are farther from each other along the bilayer normal in LC-rich systems than in a pure system. This is indicative of the lipid headgroup tilt which is defined by the angle that a vector connecting a negatively charged phosphorus and a positively charged nitrogen atoms makes with the bilayer normal (see next section for discussion). In addition, the overall density of lipids decreases throughout the range with increasing LC concentration. The value of the minimum in the total density profile follows the same trend, whereas the total density in the regions between the lipid headgroups and methyl trough is slightly higher than that observed in a pure bilayer. At the same time, the average area per lipid stays approximately constant (a systematic increase observed for high LC concentration stays within the statistical error). Therefore, the volume freed by the lipid chains through a lower degree of interdigitation and higher ordering (refer to Fig. 9 and the discussion in the following section) is now occupied by mesogens. On average, they do not make up the density loss in the methyl trough, but they do overcompensate for it in the rest of the hydrophobic part of the bilayer. Finally, as is evidenced in Fig. 8 and Table 5, the width of the water-lipid interface increases by ~0.2 nm for all LC concentrations. This effect is in contrast to the sharper interface observed in the simulations of various phospholipid bilayers with cholesterol (8–13). A wider interface in our

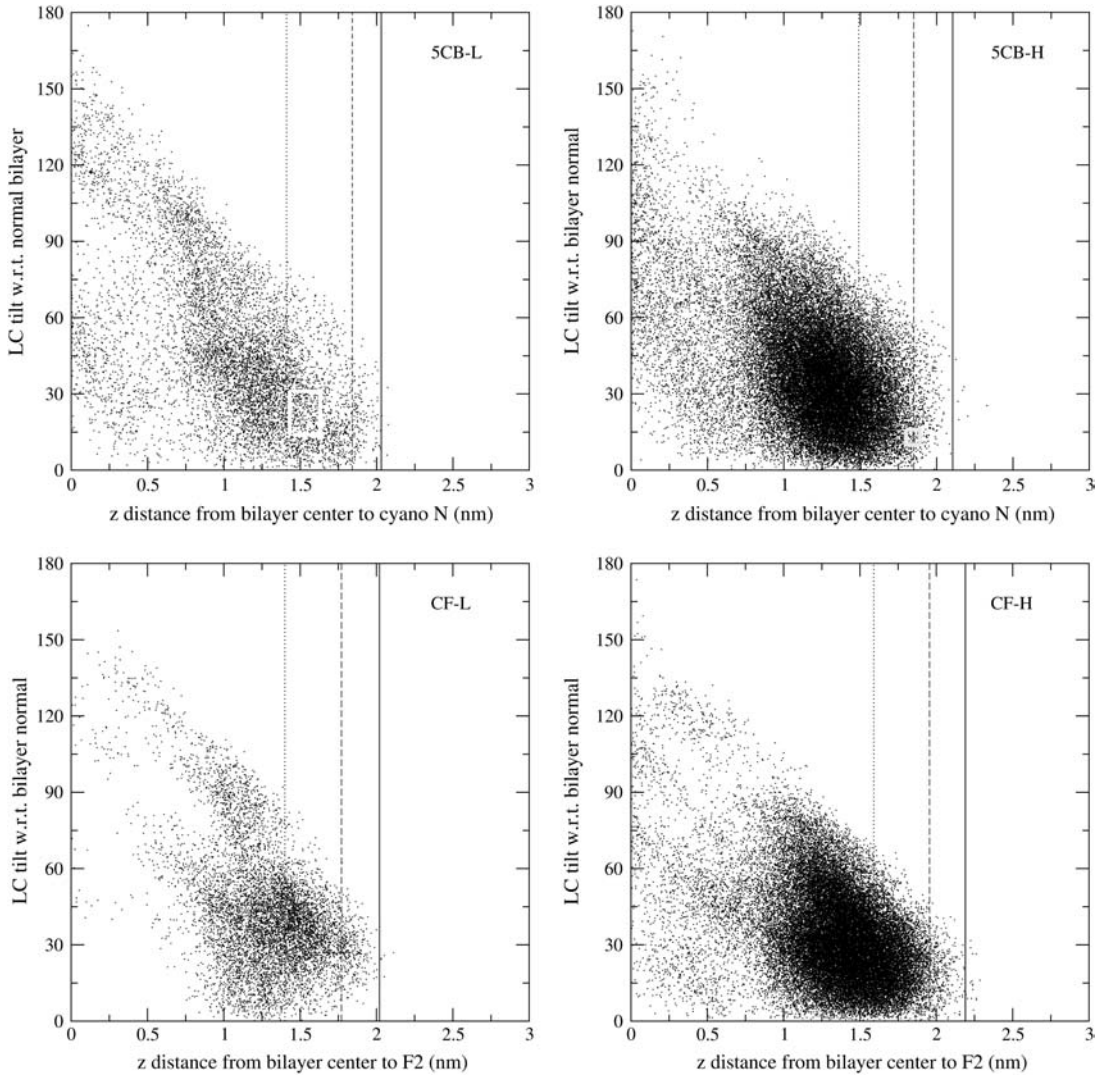

FIGURE 7 Map of the orientations that mesogens adopt depending on the position of the polar head atoms (cyano N or F2) relative to the middle of the bilayer. Relative positions of lipid nitrogen (*solid line*), phosphorus (*dashed line*), and carbonyl oxygens (*dotted line*) are also shown. The highlighted rectangles in the two upper panels indicate the range of the angles cholesterol molecules make with the bilayer normal as a function of the position of the hydroxyl group in the simulations of Smondyrev et al. (9) at 11 mol % (*upper left*) and at 50 mol % (*upper right*).

systems points to a better hydration of the lipid headgroups and, possibly, a more ''leaky'' membrane.

Structural changes in the phospholipid bilayer

In this section, we examine in more detail the structural changes undergone by lipid molecules, i.e., the tilt and the order parameter of lipid aliphatic chains and the structure within the headgroup region, in response to the inclusion of liquid crystals in the membrane.

The deuterium order parameter is defined as $S_{CD} = \langle 3\cos^2\alpha - 1\rangle/2$, where the brackets denote an average over molecules and time and α is the angle between the bilayer normal and reconstructed carbon-deuterium bonds (15). This quantity provides a measure of the alignment of lipid chains with the bilayer normal. In experiments, it can be measured using NMR spectroscopy (50). S_{CD} is plotted in Fig. 9 and compared to results for a pure bilayer at the same temperature (4). In general, we see an ordering induced by the liquid crystal, which is similar to that induced by cholesterol (8–13). Even at low concentrations, CF orders chains more effectively than 5CB, due to its longer rigid body. At high concentrations, both mesogens align the chains significantly.

In addition to the order parameter, it is useful to estimate the tilt of the lipid chains, which is defined as the angle that a vector connecting carbonyl and terminal carbons makes with the bilayer normal. Consistent with the increase in S_{CD} at higher LC concentration, the distribution of angles assumed by the lipid chains becomes narrower, and the average tilt angle decreases from 34.2° to 29.6° and 28.4° for

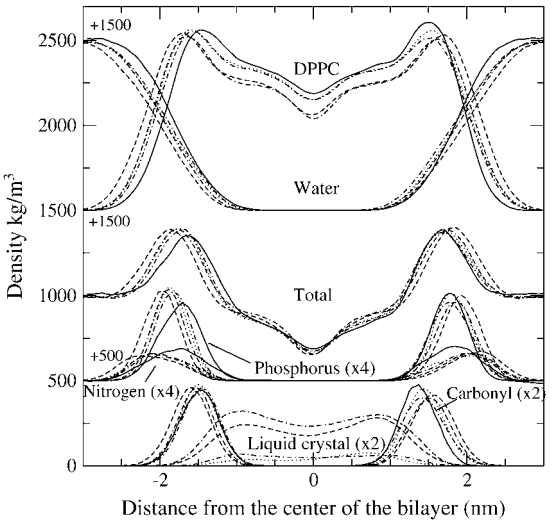

FIGURE 8 Comparison of density profiles of specific components in the LC-rich and pure bilayer systems: pure (*solid lines*), 5CB-L (*dotted lines*), CF-L (*dash-dotted lines*), 5CB-H (*dashed lines*), and CF-H (*double-dash-dotted lines*). Nomenclature is as defined in Table 1.

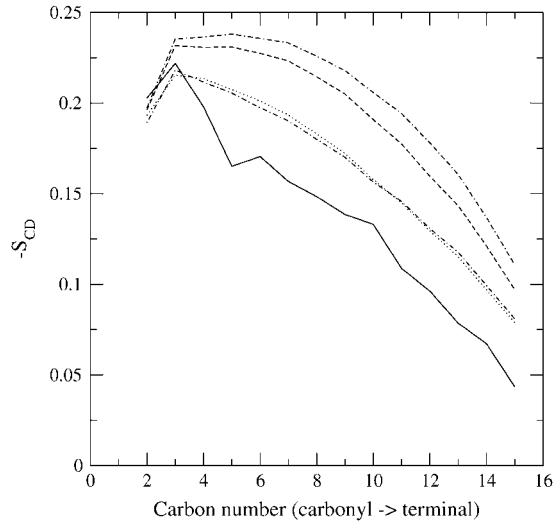

FIGURE 9 Order parameter S_{CD} for phospholipid chains: pure (*solid line*), 5CB-L (*dotted line*), CF-L (*dash-dotted line*), 5CB-H (*dashed line*), and CF-H (*double-dash-dotted line*). C1 belongs to the lipid carbonyl group, whereas C16 is the terminal carbon of the lipid chain.

the 5CB-H and CF-H systems, respectively (refer to Fig. 17). The distribution is narrower than in the case of a pure bilayer. For comparison, we also show in Fig. 10 the distributions of tilt angles adopted by LC molecules in the bilayer. The orientations of 5CB and CF molecules can be defined by a vector connecting the C8 carbon and the cyano nitrogen (CN vector), and by a vector connecting C21 and F2 (CF vector), respectively. As with the tilt of the lipid chains, the distribution becomes narrower with higher LC concentration, and the orientation of the lipids and mesogens coincide to within 7–10°. The average orientation of the lipid chains is clearly influenced by the presence of the LC.

Fig. 11 shows pair correlation functions between the nitrogen and phosphorus atoms of the lipid headgroups. In the pure bilayer, the first three peaks in $g_{PP}(r)$ are well defined and correspond to a distorted square packing (4). In the presence of LCs, the positions of the maxima remain the same but their intensity and definition decrease with increasing LC concentration. The structure between nitrogen atoms, however, is smeared out and, on average, the closest neighbors are slightly farther than in a pure bilayer, i.e., the first maximum moves from 0.71 nm to 0.84 nm. This change also takes place in a pure bilayer when the temperature is lowered to 250 K and the membrane undergoes a transition to a gel phase (4). Phosphate groups pack in the same (although less defined) way as in a pure bilayer, whereas choline groups behave differently and consistently with the structure expected for a gel phase.

TABLE 5 Average distances between the density peaks of selected atoms in lipid headgroup, lateral area, and the width of a water-lipid interface

System	d_{PP}	d_{NN}	d_{DPPC}	d_{OCOC}	Interface	Area
pure	35.2 ± 0.4	36.4 ± 0.4	29.5	28.5 ± 0.4	10.3	66.8 ± 0.5
5CB-L	36.5 ± 0.4	39.0 ± 0.5	30.6	29.3 ± 0.4	12.4	65.4 ± 1.0
CF-L	36.2 ± 0.5	39.1 ± 0.6	30.9	29.3 ± 0.5	12.5	66.1 ± 0.9
5CB-H	37.9 ± 0.4	40.9 ± 0.5	32.8	30.8 ± 0.4	12.2	67.1 ± 0.9
CF-H	38.4 ± 0.5	41.3 ± 0.5	33.5	31.4 ± 0.5	12.5	67.3 ± 1.1

Distances are given in Å. The area is defined as the average lateral area divided by a number of lipids. Interface width is calculated as a distance over which water density drops from 90% to 10% of the bulk value.

The interactions of water oxygen (O_W) with the lipid headgroups also change in the presence of LC molecules. The radial distribution functions of O_W with nitrogen, phosphorus, and carbonyl oxygen O_C shown in Fig. 12 indicate disappearance of correlation beyond a second peak (the third one in the case of O_C) and small shifts of the second (and third) peak for all pairs. The ordering of water beyond a first solvation shell observed in a pure bilayer is suppressed in the LC-rich systems. The height of the nearest neighbor peak increases with LC concentration; this is also reflected by a higher number of water molecules in the first solvation shell for phosphate and choline groups (Table 6) and is consistent with a thicker lipid-water interface.

The distribution of the orientations assumed by the phosphorus-nitrogen (PN) vector of the lipid headgroups with the bilayer normal is plotted in Fig. 13. The average angle decreases from the pure bilayer case, where the headgroups lie almost flat (average tilt of 80.2°), to the LC-rich systems, where choline groups protrude more into the water phase. This is also consistent with a higher separation between the phosphorus and nitrogen density peaks. It is interesting to compare the effect of LC with that observed by Smondyrev and Berkowitz for DPPC bilayers with 50 mol % cholesterol and 50 mol % cholesterol sulfate (9,10). The orientation of the lipid headgroups changed from 81° for a pure bilayer to 72° and 82° for cholesterol and cholesterol sulfate systems,

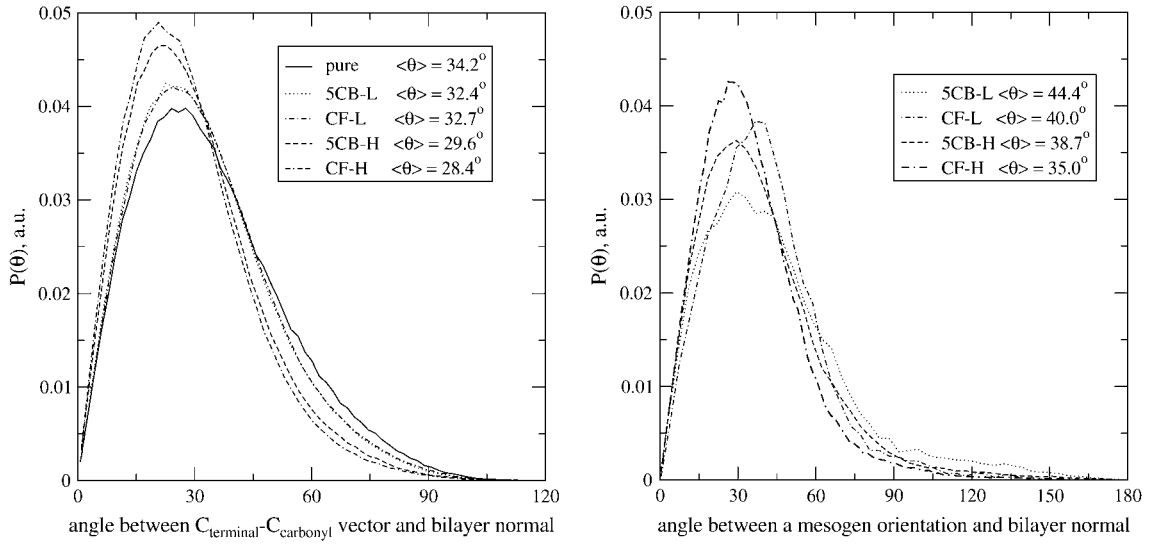

FIGURE 10 (*Left*) Phospholipid chain tilt defined by the angle between carbonyl-terminal carbon vector and the bilayer normal. (*Right*) Distribution of the orientations adopted by mesogens. Phospholipid group represented: pure (*solid line*), 5CB-L (*dotted line*), CF-L (*dash-dotted line*), 5CB-H (*dashed line*), and CF-H (*double-dash-dotted line*).

respectively. In our simulations, the incorporation of the mesogens at only 20 mol % resulted in the average PN tilt angles of 65.3° and 65.4° for 5CB and CF, respectively. Therefore, the reorientation of lipid headgroups induced by the presence of CF and 5CB is at least similar to (and possibly stronger than—our temperature is 27 K higher) that induced by cholesterol. We investigate this phenomenon further by inspecting closely specific interactions between mesogens and lipid molecules and considering the electrostatic potential across the membrane in the following section.

Specific interactions of LC molecules with lipids

Spatial correlation functions between LC molecules in the concentrated systems are plotted in Fig. 14. The data clearly indicate that the degree of correlation is much higher for 5CB molecules. A significant peak at 0.4 nm suggests that 5CB exhibits a tendency to segregate within a bilayer. In contrast, a relatively small peak is observed for CF at 0.35 nm.

The positions of selected atoms relative to the cyano N of 5CB and F2 of CF are shown in the right panel of Fig. 14 for concentrated systems. There is a slight correlation with water oxygen (peak location at $<$0.35 nm) for both mesogens. Although the cyano N can form hydrogen bonds with water, the extent of hydrogen bonding is negligible ($\approx$0.01 H bonds per configuration). In both cases, there is a peak with the choline N at 0.38 nm for 5CB and at 0.4 nm for CF; two peaks with the lipid P at $\approx$0.6 nm and 0.78 nm; and two peaks with the carbonyl oxygens of both *sn*-1 and *sn*-2 lipid acyl chains at 0.37 nm and 0.65 nm, respectively. The peaks with choline and phosphate groups indicate molecular association between mesogens and lipid headgroups. This is expected, since the choline group, which carries a positive charge, is attracted to both the cyano N in 5CB and the fluorines in CF that are negatively charged. In Fig. 15 we show the fraction of the time that a mesogen is ''associated'' with one or more lipids. We consider that association took place when the distance from the cyano N or F2 to a choline group was within the first minimum in the corresponding spatial correlation function. We found that the majority of this type of association involves one mesogen and up to three lipids. For the 5CB-H and CF-H systems, respectively, there are 12.6 and 15.4 ''bonds'' with a single lipid, 0.62 and 1.2 bonds with two lipids, and 0.01 and 0.17 bonds with three lipids per time step of the simulation. The ability to associate with more than one lipid simultaneously is enhanced in CF because of the presence of a second fluorine F4. (Although not shown, the $g(r)$ of F4 with the choline N has two peaks at 0.42 nm and 0.63 nm, both smaller than in the F2 $g(r)$.)

Typical configurations of the molecules involved in mesogen-lipid associations are shown in Fig. 16. In the case of CF, we show an instance in which a CF molecule is ''bonded'' to three lipids simultaneously: note how the F2 atom is $\sim$0.4 nm away from two choline groups on the left and $\sim$0.6 nm from the one on the right, whereas the situation is reversed for the F4 atom which is closest to the choline N on the right and farther from the ones on the left. The lifetime of mesogen-lipid associations can be as long as several nanoseconds. Thus these associations may affect the dynamics of the lipids and the LC.

Another effect of the specific interactions between LC and lipids is the local change in the orientations of the lipid headgroups. Consider the inset of Fig. 13, where the average angle of the PN vector with the bilayer normal is plotted as a function of the projected distance between the cyano N or

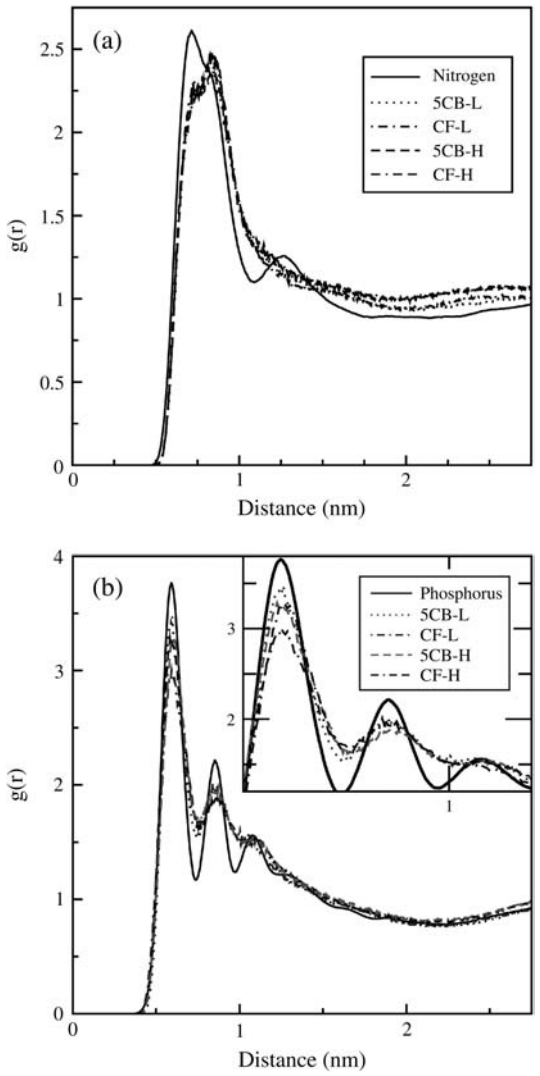

FIGURE 11 Radial distribution functions for nitrogen (*a*) and phosphorus (*b*) atoms in phospholipid headgroups: pure (*solid line*), 5CB-L (*dotted line*), CF-L (*dash-dotted line*), 5CB-H (*dashed line*), and CF-H (*double-dash-dotted line*).

F2 with the choline N onto the *xy* plane, d_{xy}. In construction of this graph, only mesogens in the lipid-water interface (i.e., either the cyano N or F2 sites that were within 0.6 nm of the average *z*-positions of choline N) were considered. It is apparent that the PN dipoles are ''pulled into'' the interface due to the electrostatic attraction between negative cyano N and fluorine atoms and positive choline nitrogens in the associated state (as also evidenced by the configurations in Fig. 16). In the vicinity of the mesogen headgroups (i.e., $d_{xy} \sim 0$), the angle between the bilayer normal and the PN vector is higher than the average and, in fact, is closer to the average angle in a pure bilayer. For distances $>\sim 0.5$ nm the local effect disappears. Note that the largest perturbation is induced in a simulation of six 5CB molecules. In this case, the PN vector of a lipid headgroup close to a cyano N lies flat on an interface. This effect is pronounced enough to affect

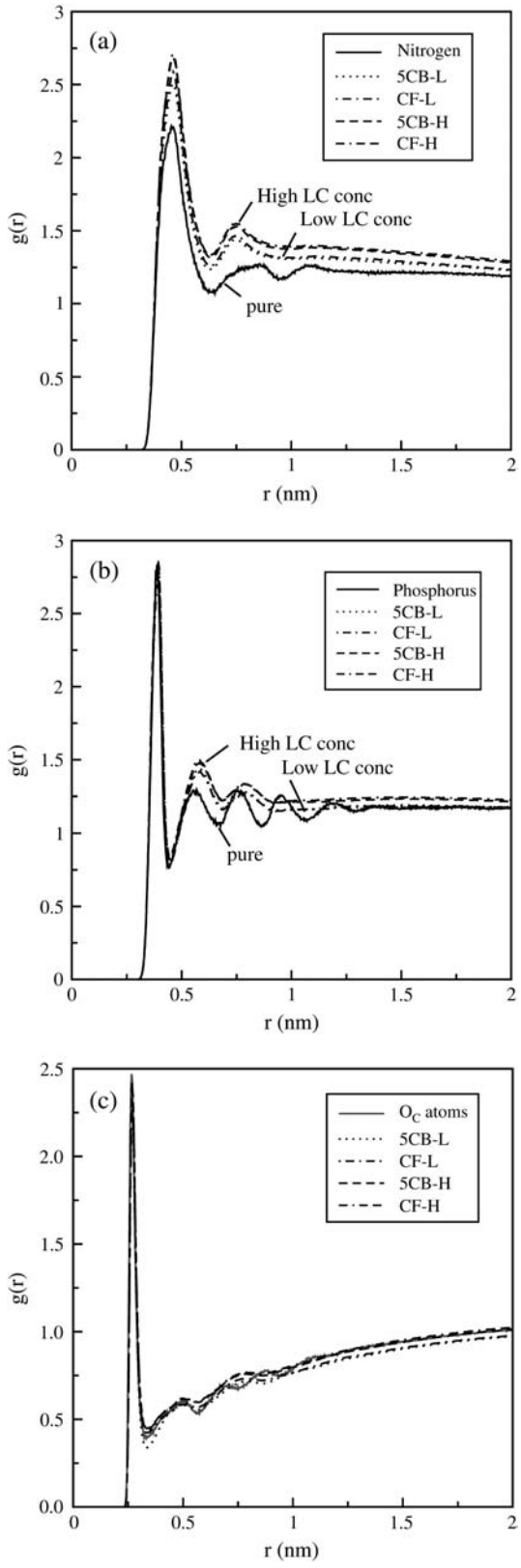

FIGURE 12 Radial distribution functions between water oxygen O_W with (*a*) nitrogen, (*b*) phosphorus, and (*c*) carbonyl oxygen O_C atoms of the phospholipid molecules: pure (*solid lines*), 5CB-L (*dotted lines*), CF-L (*dash-dotted lines*), 5CB-H (*dashed lines*), and CF-H (*double-dash-dotted lines*).

TABLE 6 Average hydration number for choline N, phosphate P, and carbonyl oxygens O_C in the lipid headgroup

System	Choline	Phosphate	Carbonyl oxygen*
pure	19.38	4.12	1.02/1.42
5CB-L	20.13	4.77	1.02/1.54
CF-L	20.49	4.67	0.97/1.72
5CB-H	20.71	4.68	1.00/1.77
CF-H	20.59	4.76	0.98/1.72

Hydration number is defined by the number of water molecules in the first solvation shell. Hydrogen bond criteria include the oxygen-oxygen distance <0.35 nm and the O-H···O angle at >120° (53).
*Values given as *sn*-1/*sn*-2.

the average PN tilt (see Fig. 13). This reorientation of the lipid headgroups is similar to the local effects of monovalent salts on a POPC bilayer described recently by Sachs et al. (51). Also note that the reorientation of the lipid headgroups next to a mesogen provides an additional stabilizing effect on the bilayer structure. An insertion of a rigid cylindrical body (i.e., a mesogen) that spans a half-width of the hydrophobic interior of the bilayer and extends just below the lipid headgroup region reduces the volume accessible to the lipid chains on one hand and, on the other, creates a ''hole'' in the lipid headgroup region. The cross-sectional area of the cylinder is ~0.40 nm^2, which is substantial when compared to the calculated area/lipid of 0.67 nm^2. Covering up the hole would minimize exposure of the hydrophobic interior to water. This mechanism then works in concert with the electrostatic interactions.

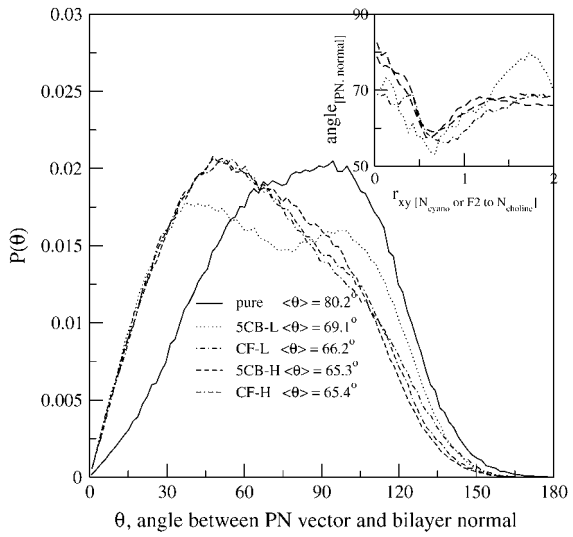

FIGURE 13 Distribution of the angle between a PN (P = phosphorus, N = nitrogen of lipid headgroups) vector with bilayer normal: pure (*solid line*), 5CB-L (*dotted line*), CF-L (*dash-dotted line*), 5CB-H (*dashed line*), and CF-H (*double-dash-dotted line*). (*Inset*) Dependence of the angle between a PN vector and the bilayer normal as a function of the distance between choline nitrogen and cyano N or F2 atoms of the mesogens projected onto the *xy* plane. The legend is the same as in the main plot.

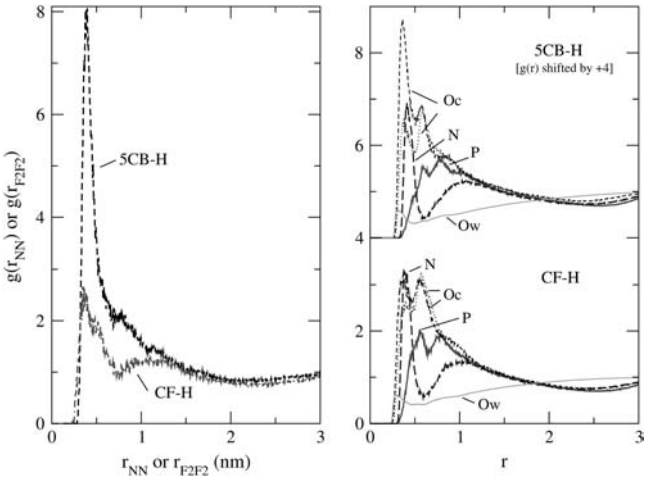

FIGURE 14 (*Left*) Spatial correlations between mesogen polar atoms: N for the 5CB-H system (*dashed line*) and F2 for the CF-H system (*double-dash-dotted line*). (*Right*) Radial distribution functions for a mesogen polar atom (N for 5CB and F2 for CF) with DPPC atoms: N (*long-dashed lines*), P (*solid lines*), *sn*-1 O_C (*short-dashed lines*), and *sn*-2 O_C (*dotted lines*); and with water oxygen O_W (*solid lines*).

In view of the above discussion, it is of interest to assess the effects of the mesogens on the electrostatic potential across the membrane. We plot the total electrostatic potential for all four systems and individual contributions from water, mesogens, and lipid headgroups and ester groups in Fig. 17; the potential is arbitrarily set to zero in the middle of the water layer, i.e., $\psi(z = 0) = 0$ and is calculated from

$$\psi(z) - \psi(0) = -1/\varepsilon_0 \int_0^z dz' \int_0^{z'} \rho(z'')dz'', \qquad (1)$$

where $\rho(z)$ is the charge density at depth z and ε_0 is the dielectric permittivity of vacuum. It is apparent from Fig. 17 that the total potential in the middle of the bilayer is always higher in the presence of CF (~780 mV for CF-H) than of 5CB (~710 mV for 5CB-H), despite the lower dipole moment of the former. To better understand this result, we examine the individual contributions from the system's components. First, the water contribution has a large positive value of 5.7 V (6.0 V) for the 5CB-H (CF-H) system. Second, the contributions of mesogens are small relative to water, but nonetheless positive distinct values of 0.4 V for 5CB and 0.2 V for CF—here we do see that 5CB generates a higher electrostatic potential than CF, in agreement with its higher dipole moment. All the negative contributions come from the lipid ester groups and headgroups. This can be readily understood in light of the discussion on the reorientation of the lipid PN vector: the presence of mesogens increases the probability of finding a PN vector directed toward the water phase, and it decreases the average tilt angle from 80° in the pure bilayer (almost parallel to the bilayer surface) to 65.3° and 65.4° in 5CB-H and CF-H, respectively. As the PN dipole is better aligned with the bilayer normal, it makes a higher contribution to the total potential.

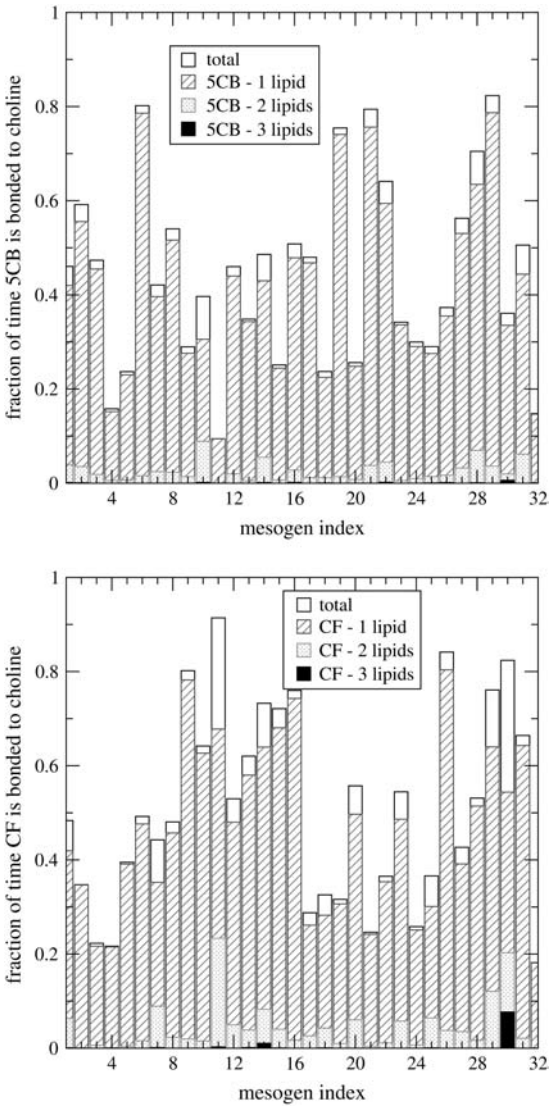

FIGURE 15 Extent of associating with lipids for 5CB-H (*top*) and CF-H (*bottom*) systems. Association takes place when N_{5CB}–N_{DPPC} or $F2_{CF}$–N_{DPPC} distances are within the first shell in radial distribution functions.

Similar effects were reported by Smondyrev et al. (9,10) in their simulations of DPPC bilayers with cholesterol: the total electrostatic potential increased from ~600 mV for a pure bilayer to ~1000 mV at a 50 mol % concentration of cholesterol, whereas the potential was not affected by the presence of 11 mol % of cholesterol. Again, due to the differences in temperature (323 K vs. 350 K in this work) and force fields, we cannot compare these results directly. Nonetheless, the signs of the individual contributions, including that of cholesterol, are consistent with our results and the actual values of the potentials are in the same range, e.g., a water contribution of ~500 mV.

CONCLUSIONS

We have conducted two types of molecular dynamics simulation to elucidate the interactions of mesogens with

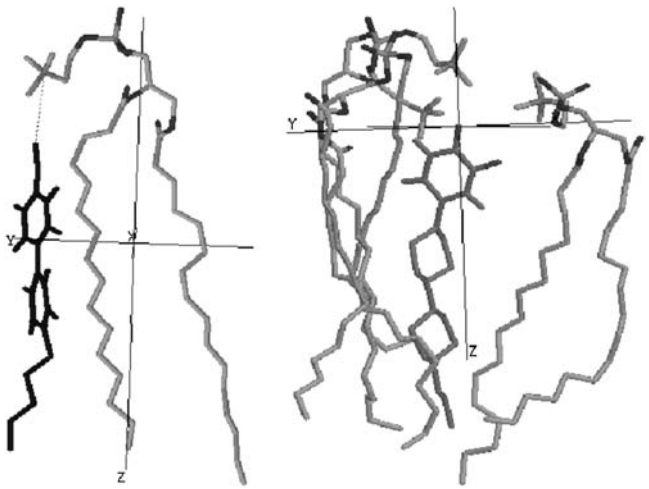

FIGURE 16 Association of 5CB (*left*) and CF (*right*) with lipids.

phospholipid bilayers. In the first type, we have performed a series of umbrella sampling simulations where a selected mesogen site was constrained, to sample a range of penetration depths in the bilayer. From these, we have provided an estimate of the PMF on the mesogen as a function of its distance from the bilayer center. Simulations of an individual 5CB or 5CF molecule in a DPPC bilayer indicate that the free energy changes for the transfer of a mesogen from the aqueous to the lipid phase (i.e., $-18\ k_BT$ and $-26\ k_BT$ for 5CB and 5CF, respectively) are highly favorable, with a small energy barrier of $\sim 0.3\ k_BT$ associated with the initial insertion of a mesogen's aliphatic tail into the bilayer. These results suggest that, at equilibrium, mesogens partition into the membrane. At lower temperatures, comparable to those at which experimental data are available, the shape of the PMF may change; in particular, one may expect a higher energy barrier at the water-lipid interface due to a reduced lipid motion and higher resistance to permeation.

The DSC analysis of pure DPPC vesicles in water exposed to a bulk liquid crystal reveals an appreciable amount of 5CB in the lipid phase after a week of exposure at room temperature, whereas a negligible amount of 5CF is detected in the vesicles after the same exposure. At the same time, the solubility of 5CB in water is of the order of μM, whereas it is undetectable (by UV absorbance) for 5CF at the same conditions. These observations, combined with the simulation results for favorable partition energies (almost 1.5 times lower for 5CF as for 5CB), lead us to the conclusion that it is the mesogen's solubility in water that controls the permeation process.

Relatively long (20-ns) simulations of DPPC bilayers with 5CB or a 50/50 mixture of 5CF and 3CF emulate experimental investigations by DSC of fully hydrated DPPC vesicles with LC incorporated at a range of concentrations; the highest (20 mol %) and the lowest (4.5 mol %) correspond to the concentrations studied in this work. It is more difficult to

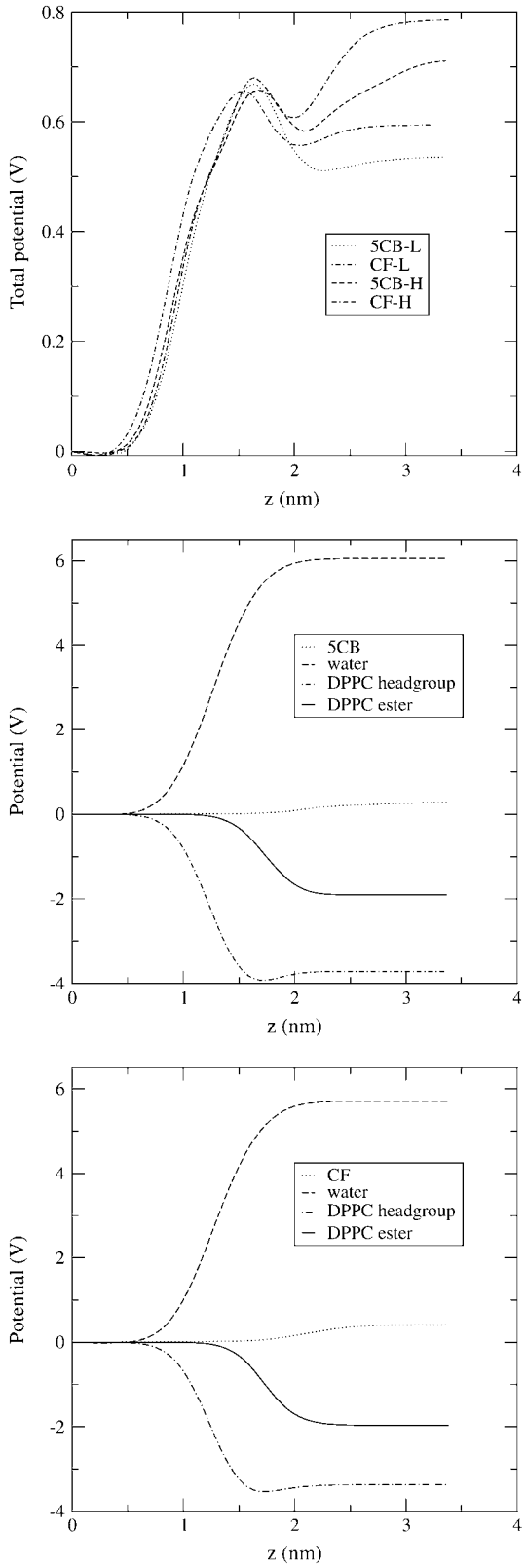

FIGURE 17 Electrostatic potential across the membrane. (*Top*) Total potential for all systems: 5CB-L (*dotted lines*), CF-L (*dash-dotted lines*), 5CB-H (*dashed lines*), and CF-H (*double-dash-dotted lines*). (*Middle and Bottom*) Breakdown of contributions from mesogens (*dotted lines*), water (*dashed lines*), lipid headgroups (*dash-dotted lines*), and ester groups (*solid lines*) for 5CB-H (*middle*) and CF-H (*bottom*) systems. Note that $z = 0$ refers to the middle of the water layer.

compare our simulation results to experiments as the latter mainly provide information on the changes in the pretransition and main transition conditions between the ordered gel and the disordered liquid crystalline phases. In particular, the DSC analysis reports a decrease in the main transition temperature and significant broadening of the transition region. In these experiments, 5CB seems to affect the bilayer structure and physical properties to a larger extent than CF. As reported by Kühnau et al. (24), the size of the cooperative units of phospholipids is reduced upon incorporation of 5CB into vesicles. An additional possibility is that the membranes become more inhomogeneous in the presence of 5CB—this is reflected by the broadened transition region.

In our simulations, we observe higher ordering of the lipid chains and close alignment (within 10°) with the mesogens, a decrease in the average tilt of the lipid headgroups, and thickening of the membranes. Finally, specific associations between a mesogen and up to three neighboring lipids were observed; they last on the order of nanoseconds and affect the lateral motion of the lipids. All the effects are more noticeable with increasing concentrations of LC and are more pronounced for CF than for 5CB. On the other hand, we observe a higher propensity to self-aggregate and a larger range of orientations sampled by molecules in the case of 5CB compared to CF. This difference in the mesogens' behavior could, perhaps, be enhanced at lower temperatures in the transition range and result in broader DSC thermograms for 5CB.

It is also of interest to compare the effects of cholesterol on a DPPC bilayer investigated by previous simulations (7) with the effects of 5CB and CF. For the former, a condensing effect (i.e., a smaller area/lipid and enhanced lipid chain ordering in the L_α phase) has been demonstrated. Also, a decrease in the angle that a PN vector of a DPPC headgroup makes with the bilayer normal in the presence of cholesterol has been observed. Although the change in the lipid headgroup tilt angle and the increased tail ordering have been observed in our simulations as well, we did not find significant changes in the lateral area of the lipids.

Another interesting aspect of the interactions between mesogens and bilayers is the change in the elastic properties of the membranes associated with the incorporation of mesogens. Phospholipid membranes are two orders of magnitude more compliant than globular proteins and, for that matter, mesogens. When a protein partitions into the membrane, the latter thins or thickens to match the hydrophobic length of a protein. Due to the induced elastic stress within a membrane, it mediates the interactions between the embedded proteins (that otherwise would be of hard-core character) and is responsible for aggregation of proteins or isolation of the regions within the membrane with different

properties, e.g., stiffness, thickness, concentration of protein, etc. (49). The question would be whether the mesogens considered in this work are sufficiently long to induce such changes in a membrane. To answer this question, much larger systems must be considered due to the longer range of elastic interactions. To make this problem tractable, coarse-graining of the components of a bilayer system would be necessary. Finally, it is instructive to compare the results for 5CB and CF in this article with the results obtained by Repakova et al. (52) for 1,6-diphenyl-1,3,5-hexatriene (DPH), a fluorophore commonly used in studies of lipid membranes. The authors used equilibrium molecular dynamics simulation to investigate the behavior of DPH upon its inclusion in DPPC bilayer at 1:128 and 3:128 DPH/DPPC ratios. DPH is a rigid, linear, rod-like molecule 1.355 nm long (i.e., two phenyl rings connected by an aliphatic six-carbon chain featuring three consecutive double bonds) and thus is similar to the molecules investigated in this article. Like 5CB and CF, DPH preferentially resides in the hydrophobic part of the membrane below the lipid headgroups interspersed with lipid acyl chains and does not partition into the methyl trough. Furthermore, it aligns closely with the bilayer normal (average angle of 25°) and rarely is found to be parallel to the bilayer plane. The authors found, on average, one flip-flop event per 100 ns per DPH molecule. This rate is higher than that reported for cholesterol (in fact, cholesterol has not been observed to flip in up to 100 ns of simulation time) but still lower than that of the mesogens in this work (it would be good to calculate what rate we have for 5CB and CF). Slight thickening ($\sim$0.06 nm that amounts to a 2% increase) of the membrane and an insignificant (within the error bar) increase in the area were observed. Although the latter is true for lipid-mesogen systems, the width of the bilayer, or rather distances between various lipid atoms belonging to lipid headgroups, seems to be affected to a much higher extent by mesogens. This is undoubtedly due to specific interactions between the polar atoms on 5CB and CF. Unlike 5CB and CF, DPH does not have any polar atoms and therefore does not interact with lipid headgroups. As a result, the angle between the PN vector and bilayer normal remains unchanged from that in a pure bilayer. Interestingly, DPH does not show any tendency toward self-aggregation, much like the less polar CF molecule. The studied concentrations of DPH in the bilayer (52), however, were considerably lower than the ones investigated in this work. In general, we find an agreement with the work of Repakova et al. for the results where the charges on the molecules play no role.

The authors are greateful to S. Ohtake, C. Schebor, and R. Riggleman for helpful discussions, to M. Wilson and D. Cheung for providing the details of the force field for mesogenic compounds, to M. Biddy for assisting with force field related calculations, and to A. Sum for providing the details of previous simulations.

This work has been supported by the University of Wisconsin Materials Research Science and Engineering Center on Nanostructured Materials and Interfaces (NSF-DMR-0520527).

REFERENCES

1. Mukhopadhay, P., H. J. Vogel, and P. D. Tieleman. 2004. Distribution of pentachlorophenol in phospholipid bilayers: a molecular dynamics study. *Biophys. J.* 86:337–345.
2. MacCallum, J. L., P. Mukhopadhay, H. Luo, and D. P. Tieleman. 2003. Large scale molecular dynamics simulations of lipid-drug interactions, in Senechal, D. 2003. Proc. 17th Annual International Symposium on High Performance Computing Systems and Applications and the OSCAR Symposium. NRC Research Press, Ottawa, Canada.
3. Lee, B., W. R. Faller, A. K. Sum, I. Vattulainen, M. Patra, and M. Karttunen. 2004. Structural effects of small molecules on phospholipid bilayers investigated by molecular simulations. *Fluid Phase Equilibr.* 225:63–68.
4. Sum, A. K., R. Faller, and J. J. de Pablo. 2003. Molecular simulation study of phospholipid bilayers and insights of the interactions with disaccharides. *Biophys. J.* 85:2830–2844.
5. Villarreal, M. A., S. B. Díaz, E. A. Dislavo, and G. G. Montich. 2004. Molecular dynamics simulation study of the interaction of trehalose with lipid membranes. *Langmuir.* 20:7844–7851.
6. Sum, A. K., and J. J. de Pablo. 2003. Molecular simulation study on the influence of dimethylsulfoxide on the structure of phospholipid bilayers. *Biophys. J.* 85:3636–3645.
7. Smondyrev, A. M., and M. L. Berkowitz. 1999. Molecular dynamics simulation of DPPC bilayer in DMSO. *Biophys. J.* 76:2472–2478.
8. Tu, K., M. L. Klein, and D. J. Tobias. 1998. Constant-pressure molecular dynamics investigation of cholesterol effects in a dipalmitoylphosphatidylcholine bilayer. *Biophys. J.* 75:2147–2156.
9. Smondyrev, A. M., and M. L. Berkowitz. 1999. Structure of DPPC/cholesterol bilayer at low and high cholesterol concentrations: molecular dynamics simulation. *Biophys. J.* 77:2075–2089.
10. Smondyrev, A. M., and M. L. Berkowitz. 2000. Molecular dynamics simulation of dipalmitoylphosphatidylcholine membrane with cholesterol sulfate. *Biophys. J.* 78:1672–1680.
11. Smondyrev, A. M., and M. L. Berkowitz. 2001. Molecular dynamics simulation of the structure of dimyristoylphosphatidylcholine bilayers with cholesterol, ergosterol, and lanosterol. *Biophys. J.* 80:1649–1658.
12. Jedlovszky, P., and M. Mezei. 2003. Effect of cholesterol on the properties of phospholipid membranes. 1. Structural features. *J. Phys. Chem. B.* 107:5311–5321.
13. Jedlovszky, P., N. N. Medvedev, and M. Mezei. 2003. Effect of cholesterol on the properties of phospholipid membranes. 3. Local lateral structure. *J. Phys. Chem. B.* 108:465–472.
14. Falck, E., M. Patra, M. Karttunen, M. T. Hyvönen, and I. Vattulainen. 2004. Lessons of slicing membranes: interplay of packing, free area, and lateral diffusion in phospholipid/cholesterol bilayers. *Biophys. J.* 87:1076–1091.
15. Tieleman, P. D., S. J. Marrink, and H. J. C. Berendsen. 1997. A computer perspective of membranes: molecular dynamics studies of lipid bilayer systems. *Biochim. Biophys. Acta.* 1331:235–269.
16. Brake, J. M., M. K. Daschner, Y.-Y. Luk, and N. L. Abbott. 2003. Biomolecular interactions at phospholipid-decorated surfaces of liquid crystals. *Science.* 302:2094–2097.
17. Fang. 2003. Imaging biological cells using liquid crystals. *Langmuir.* 19:2865–2869.
18. Skaife, J. J., J. M. Brake, and N. L. Abbott. 2001. Influence of nanometer scale topography of surfaces on the orientational response of liquid crystals to proteins specifically bound to surface-immobilized receptors. *Langmuir.* 17:5448–5457.
19. Gupta, V. K., J. J. Skaife, T. B. Dubrovsky, and N. L. Abbott. 1998. Optical amplificaton of ligand-receptor binding using liquid crystals. *Science.* 279:2077–2080.
20. Van Nelson, J. A., S.-R. Kim, and N. L. Abbott. 2002. Amplification of specific binding events between biological species using lyotropic liquid crystals. *Langmuir.* 18:5031–5035.

21. Skaife, J. J., and N. L. Abbott. 2001. Influence of molecular-level interactions on the orientations of liquid crystals supported on nanostructured surfaces presenting specifically bound proteins. *Langmuir*. 17:5595–5604.
22. Brake, J. M., and N. L. Abbott. 2003. An experimental system for imaging the reversible adsorption of amphiphiles at aqueous-liquid crystal interfaces. *Langmuir*. 18:6101–6109.
23. Luk, Y.-Y., S. F. Campbell, N. L. Abbott, and C. J. Murphy. 2004. Non-toxic thermotropic liquid crystals for use with mammalian cells. *Liq. Cryst.* 31:611–621.
24. Kühnau, U., B. Madler, S. Würlitzer, G. Rapp, and H. Schmiedel. 1997. Incorporation of thermotropic liquid crystals in phospholipid monolayers: necessary condition of homeotropic anchoring. *Mol. Cryst. Liq. Cryst.* 304:171–178.
25. Kühnau, U., A. G. Petrov, G. Klose, and H. Schmiedel. 1999. Measurements of anchoring energy of a nematic liquid crystal, 4-cyano-4′-*n*-pentylbiphenyl, on Langmuir-Blodgett films of dipalmitoyl phosphatidylcholine. *Phys. Rev. E.* 59:578–585.
26. Reference deleted in proof.
27. Luk, Y.-Y., M. L. Tingey, D. J. Hall, B. A. Israel, C. J. Murphy, P. J. Bertics, and N. L. Abbott. 2003. Using liquid crystals to amplify protein-receptor interactions: design of surfaces with nanometer-scale topography that present histidine-tagged protein receptors. *Langmuir*. 19:1671–1680.
28. Berendsen, H. J. C., D. van der Spoel, and R. van Drunen. 1995. GROMACS: a message-passing parallel molecular-dynamics implementation. *Comput. Phys. Commun.* 91:43–56.
29. Berendsen, H. J. C., J. P. M. Postma, W. F. van Gunsteren, A. DiNola, and J. R. Haak. 1984. Molecular dynamics with coupling to an external heat bath. *J. Chem. Phys.* 81:3684–3690.
30. Essman, U., L. Perera, M. L. Berkowitz, T. Darden, H. Lee, and L. G. Pedersen. 1995. A smooth particle mesh Ewald method. *J. Chem. Phys.* 103:8577–8593.
31. Berendsen, H. J. C., J. R. Grigera, and T. P. Straatsma. 1987. The missing term in effective pair potentials. *J. Phys. Chem.* 91:6269–6271.
32. van Gunsteren, W. F., S. R. Billeter, A. A. Eising, P. H. Hünenberger, P. Krüger, A. E. Mark, W. R. P. Scott, and I. G. Tironi. 1996. Biomolecular Simulation: The GROMOS Manual and User Guide. Vdf, Zürich.
33. Nath, S. K., B. J. Banaszak, and J. J. de Pablo. 2001. A new united atom force field for α-olefins. *J. Chem. Phys.* 114:3612–3616.
34. Nath, S. K., F. A. Escobedo, and J. J. de Pablo. 1998. On the simulation of vapor-liquid equilibria for alkanes. *J. Chem. Phys.* 108:9905–9911.
35. Nath, S. K., and J. J. de Pablo. 2000. Simulation of vapour liquid equilibria for branched alkanes. *Mol. Phys.* 98:231–238.
36. Neubauer, B., A. Boutin, B. Tavitian, and A. H. Fuchs. 1999. Gibbs ensemble simulations of vapour-liquid phase equilibria of cyclic alkanes. *Mol. Phys.* 97:769–776.
37. Cheung, D. L., S. J. Clark, and M. R. Wilson. 2002. Parametrization and validation of a force field for liquid-crystal forming molecules. *Phys. Rev. E.* 65:051709.
38. Lansac, Y., M. A. Glaser, and N. A. Clark. 2001. Microscopic structure and dynamics of a partial bilayer smectic liquid crystal. *Phys. Rev. E.* 64:051703.
39. Komolkin, A. V., A. Laaksonen, and A. Maliniak. 1994. Molecular-dynamics simulation of a nematic liquid-crystal. *J. Chem. Phys.* 101: 4103–4116.
40. Frisch, M. J., G. W. Trucks, H. B. Schlegel, G. E. Scuseria, M. A. Robb, J. R. Cheeseman, V. G. Zakrzewski, J. A. Montgomery, R. E. Stratmann, J. C. Burant, S. Dapprich, J. M. Millam, A. D. Daniels, K. N. Nudin, M. C. Strain, O. Farkas, J. Tomasi, V. Barone, M. Cossi, R. Cammi, B. Menucci, C. Pomelli, C. Adamo, S. Clifford, J. Ochterski, G. A. Petersson, P. Y. Ayala, Q. Cui, K. Morokuma, D. K. Malick, A. D. Rabuck, K. Raghavachari, J. B. Foresman, J. Cioslowski, J. V. Ortiz, B. B. Stefanov, G. Liu, A. Liashenko, P. Piskorz, I. Komaromi, R. Gomperts, R. L. Martin, D. J. Fox, T. Keith, M. A. Al-Laham, C. Y. Peng, A. Nanayakkara, C. Gonzalez, M. Challacombe, P. M. W. Gill, B. G. Johnson, W. Chen, M. W. Wong, J. L. Andres, M. Head-Gordon, E. S. Replogle, and J. A. Pople. 1998. Gaussian 98 Revision A.5. Gaussian, Pittsburg, PA.
41. Kumar, S., D. Bouzida, R. H. Swendsen, P. A. Kollman, and J. M. Rosenberg. 1992. The weighted histogram analysis method for free-energy calculations of biomolecules. *J. Comput. Chem.* 13: 1011–1021.
42. Bemporad, D., and J. W. Essex. 2004. Permeation of small molecules through a lipid bilayer: a computer simulation study. *J. Phys. Chem. B.* 108:4875–4884.
43. Marrink, S. J., and H. J. C. Berendsen. 1994. Simulation of water transport through a lipid membrane. *J. Phys. Chem.* 98:4155–4168.
44. Marrink, S. J., R. M. Sok, and H. J. C. Berendsen. 1996. Free volume properties of a simulated lipid membrane. *J. Chem. Phys.* 104:9090–9099.
45. Israelachvili, J. 1992. Intermolecular and Surface Forces, 2nd ed. Academic Press, San Diego.
46. Seelig, J., and P. Ganz. 1991. Non-classical hydrophobic effect in membrane binding equilibria. *Biochemistry*. 30:9354–9359.
47. Kessel, A., N. Ben-Tal, and S. May. 2001. Interactions of cholesterol with lipid bilayers: the preferred configuration and fluctuations. *Biophys. J.* 81:643–658.
48. Sitkoff, D., N. Ben-Tal, and B. Honig. 1996. Calculation of alkane to water solvation free energies using continuum solvent models. *J. Phys. Chem.* 100:2744–2752.
49. Harroun, T. A., W. T. Heller, T. M. Weiss, L. Yang, and H. W. Huang. 1999. Experimental evidence for hydrophobic matchin and membrane-mediated interactions in lipid bilayers containing gramicidin. *Biophys. J.* 76:937–945.
50. Petrache, H. I., S. W. Dodd, and M. F. Brown. 2000. Area per lipid and acyl length distributions in fluid phosphatidylcholines determined by ^{2}H NMR spectropscopy. *Biophys. J.* 79:3172–3192.
51. Sachs, J. N., H. Nanda, H. I. Petrache, and T. B. Woolf. 2004. Changes in phosphatidylcholine headgroup tilt and water order induced by monovalent salts: molecular dynamics simulations. *Biophys. J.* 86: 3772–3782.
52. Repakova, J., P. Capkova, J. M. Holopainen, and I. Vattulainen. 2004. Distribution, orientation, and dynamics of DPH probes in DPPC bilayer. *J. Phys. Chem. B.* 108:13438–13448.
53. Brady, J. W., and R. K. Schmidt. 1993. The role of hydrogen bonding in carbohydrates: molecular dynamics simulations of maltose in aqueous solution. *J. Phys. Chem.* 97:958–966.